Chapter 5

Fabrication of Lemon-CDs-Curcuminoids based Supramolecular Architecture for Development of Drug Delievery System

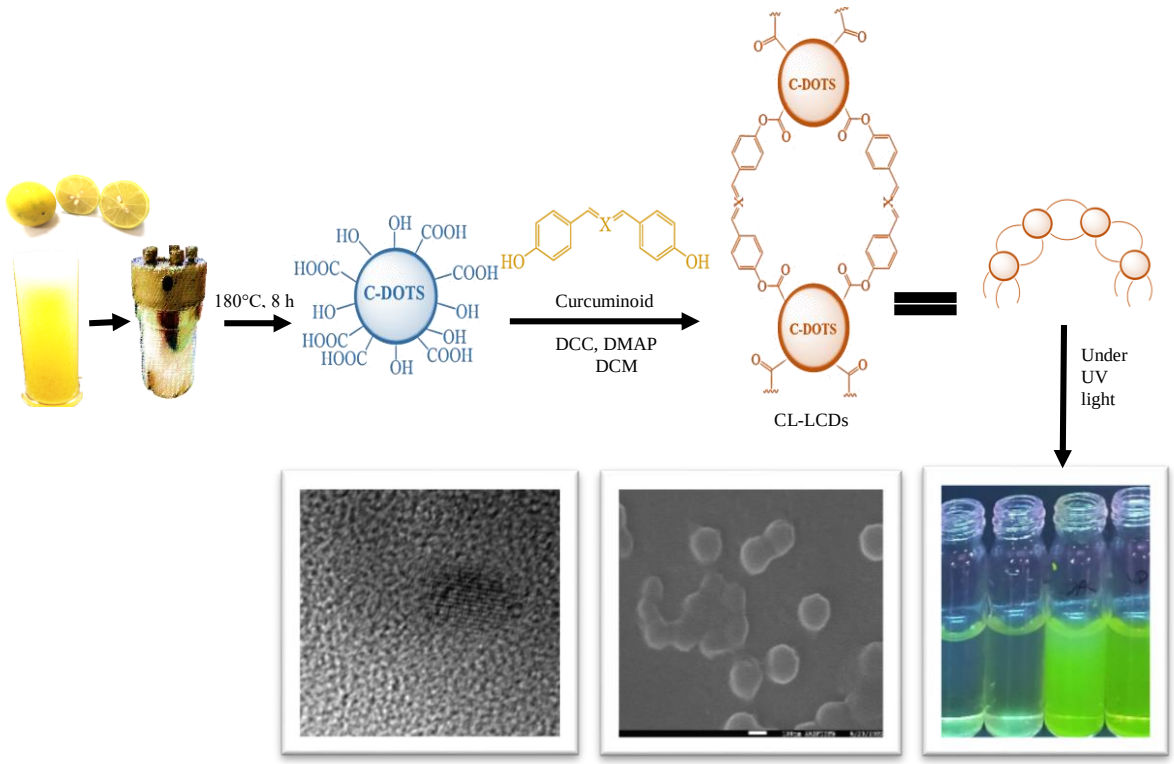

5.1. Introduction

5.1.1. Carbon Dots

A quasi-zero dimensional carbon material with a size < 20 nm, is typically referred to as a carbon dots (CDs). Fluorescence is the characteristic property of CDs[1]. Due to their excellent properties like controllable photoluminescence (PL), excellent quantum yield (QY), low toxicity, small size, notable biocompatibility, and plentiful low-cost sources, carbon dots have drawn significant attention. They have vast applications in the field of biomedicine, catalysis, optoelectronic devices, and anticounterfeiting[2-10].

The CDs are excellent candidates for development of drug delivery systems and bio imaging tools due to easy customisation like attachment of antibodies[11,12], proteins[13], natural products[14] etc.

5.1.2. Advantages of Carbon Dots [15]

- **Inexpensive**: CDs is an emerging star as a nanocarbon member since it is both affordable and abundant.
- **Photostability**: As compared to organic dyes and regular quantum dots (QDs), CDs have a higher photostability.
- **Broader excitation and narrow emission**: CDs feature a more defined emission peak and a broader excitation spectrum than organic dyes and other cadmium based quantum dots.
- **Biological properties**: CDs have exceptional biological features, such as hydrophilicity, low toxicity, chemical stability and strong biocompatibility, which ensure their potential applications in field of biosensor, drug delivery and bio-imaging.
- **Luminescence**: As compared to other QDs they have higher luminescence.
- **Aqueous stability**: In comparison to organic dyes CDs have higher aqueous stability.
- **Electronic properties**: The electrochemical luminescence and chemiluminescence are caused by the exceptional electronic characteristics of carbon based QDs as electron donors and acceptors, which gave them a wide range of applications in optronics, catalysis, and sensors.
- **Chemical inertness:** As compared to other QDs, carbon dots have higher chemical stability.

5.1.3. Methods of synthesis of Carbon dots

Two methods—the top-down method and the bottom-up method—can be used primarily to synthesise CDs.

A. Top-Down Method

The cleaving of carbonaceous materials into tiny nano-sized particles via electrochemical, chemical, or physical dissection methods is known as the top-down approach. Macroscopic carbonaceous materials, such as activated carbon, carbon nanotubes (CNTs), and graphite, are currently widely used in top-down CDs manufacturing processes, such as arc discharge, laser ablation, ultrasonic treatment, and electrochemical techniques[16,17]. Nevertheless, these methods are typically used in conditions with lots of acidity, potential, and energy. These top-down procedures are particularly time-consuming compared to bottom-up approaches because of the extreme conditions[18,19].

B. Bottom – Up Method

The bottom-up strategy involves transforming tiny carbon structures into CDs of the appropriate size. In order to create CDs, a bottom-up technique is used, which includes solvothermal method, hydrothermal method, ultrasonic method, thermal decomposition, pyrolysis, carbonization, and microwave method[20].

The CDs often have many functional groups, such as –OH, –COOH, and $–NH_2$ on their surface. Interestingly, the presence of these functional groups (amino, hydroxyl, carboxyl, etc.) on the surface of CDs depends on the precursors from which they are synthesized and contributes to their solubility in water and customized control[21].

The user-defined control enables the user to regulate the size, shape, and aggregation properties of nanoparticles for their use in various nano-biotechnology applications.

The properties of CDs can be updated and modified by selecting precursors during synthesis, surface passivation, and functionalization. Rather than creating CDs from fresh precursors, it is more important to achieve a surface modification of CDs to enhance their luminescence qualities and to create new applications. Covalent bonds are used to attach additional functional groups on the surface of the CDs, which alter the electron cloud density on their surface. This will make a change in the conjugation and alter the fluorescence spectrum of CDs. Most of the

surface of carbon dots is covered by carboxylic acid functional groups on which amide formation, silylation, esterification, sulfonylation and copolymerization reactions take place[22].

Among all the surface functionalization reaction, the esterification of carboxylic acid confers excellent selectivity and reversibility to the modified CDs towards targets, opening the door for the use of CDs in detection and cell imaging fields.

In 2014, Baruah et. al., reported CDs from citric acid that has surface carboxylic acid groups; it was shown that simple esterification of these groups with different alcohols increased the PL intensity of CDs at pH 1 and decreased it at pH 7 (figure 5.1). This revealed that PL intensity of esterified CDs is pH sensitive. This work suggest the application of esterified CDs in fluorescence-based optical switches[23].

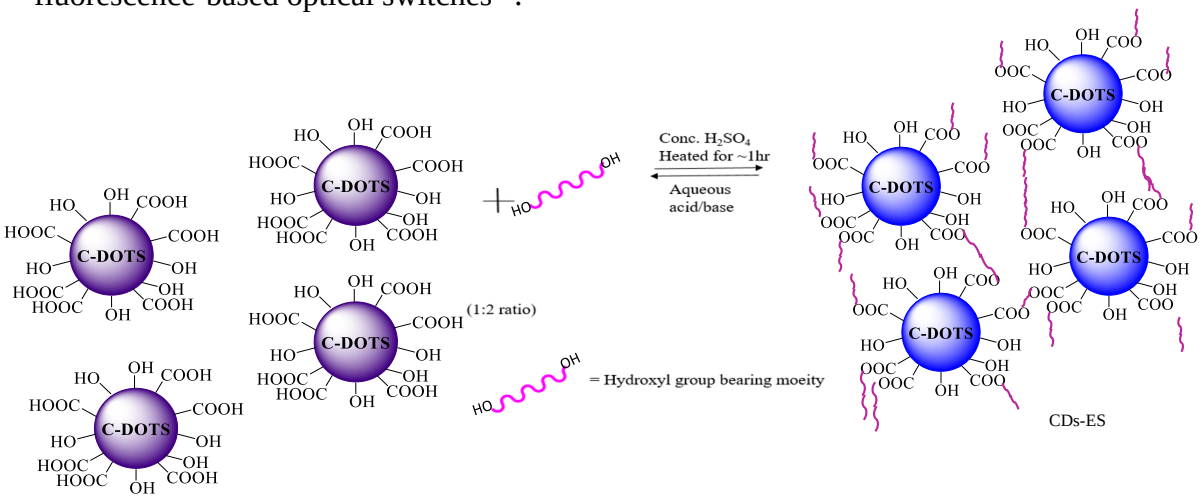

Figure 5.1. Schematic representation of the esterification process of CDs[23].

Similarly the other researcher generated flame-retardant free high-temperature-resistant textiles by esterification of CDs with various alcohol. In the presence of excess alcohol and a powerful acid catalyst, Shishodia et. al. converted carboxylic acids functionalised CDs using Fischer Esterification or Fischer-Speier Esterification, to an ester. To achieve the desired covalently esterified CDs, they added concentrated sulphuric acid in a catalytic amount to the solution of CDs and heated it for a few hours. They studied the thermal stability of esterified CDs at high temperature and found it suitable for development of high-temperature-resistant textiles[24].

Lin et. al. successfully developed spiropyran-functionalized CDs by connecting ester linkages between spiropyran and CDs. SP-CDs were able to achieve reversible blue to red colour alteration. In addition to being a strong contender for high-contrast pH sensing systems, the

dual-responsive SP-CDs displayed great performance when employed in light emitting diodes (LEDs) for illumination[25].

A novel fluorescent sensor for the detection of the environmental contaminant 2, 4, 6-trinitrophenol (TNP) in aqueous medium was developed by Gao et. al. using the esterification of CDs. They prepared the passivated CDs by heating a mixture of carboxymethyl cellulose sodium (CMC) and 4, 7, 10-trioxa-1, 13-tridecanediamine (TTDDA). Then, by means of an esterification reaction, (3-chloro-2-hydroxypropyl) trimethylammonium chloride (CTA) was chemically grafted on the surface of the passivated CDs to produce quaternary ammonium-functionalized CTA-CDs (figure 5.2)[26].

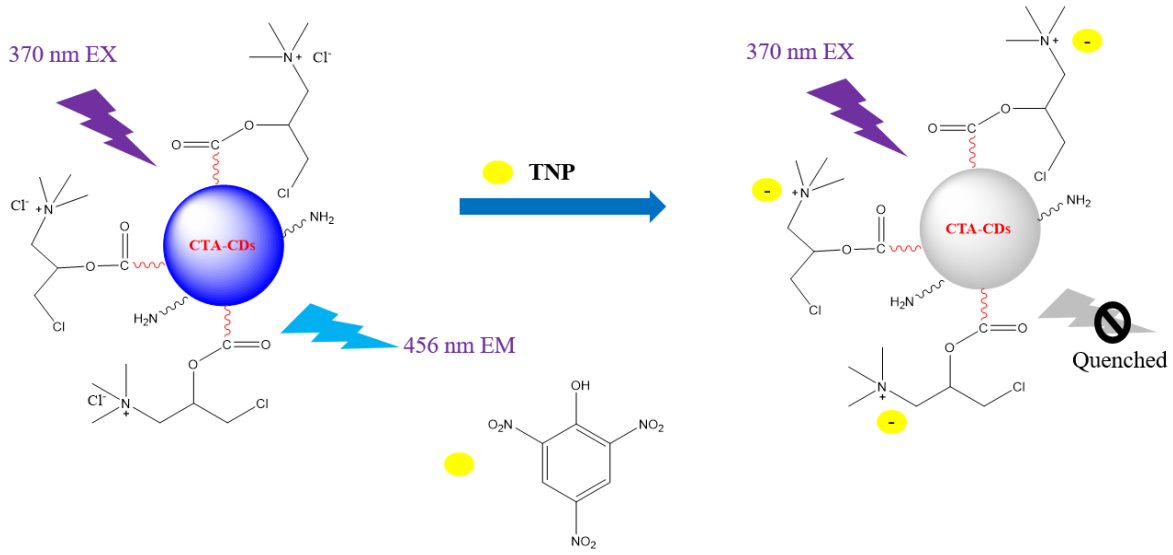

Figure 5.2. Schematic illustration for the sensitive and selective detection of TNP based on the CTA-CDs[26].

Due to the fluorescent properties of CDs the researcher also explored the application of CDs in the field of bio-labelling. Using ammonium citrate as a carbon source and folic acid/mannose molecules as recognition ligands, Lai et. al. created a CDs using solid-state synthesis. Folic acid/mannose molecules were anchored to the surface of CDs via an esterification process (figure 5.3). The resultant CDs were used to selectively label tumour cells/bacteria due to intense blue fluorescence[27].

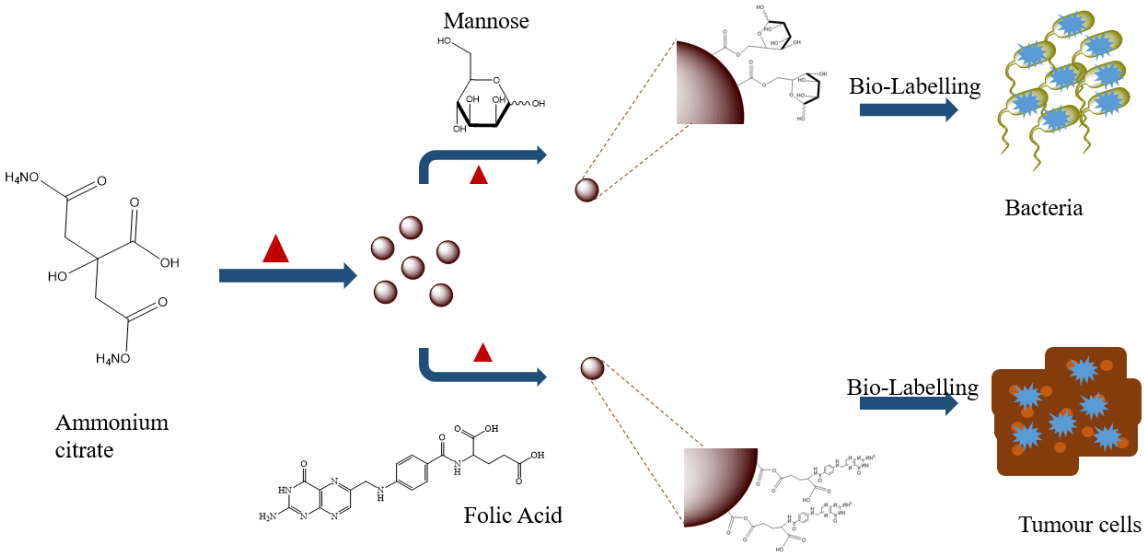

Figure 5.3. Schematic representation of mannose based CDs and folic acid based CDs for selective labelling of *E. coli* and tumour cells[27].

In a similar manner, Dilag et. al. employ the luminous CDs /p (DMA) nano-composite to find latent fingerprints on aluminium foil. They produced CDs by hydrothermally treated activated charcoal (AC) in acidic conditions, and then they conjugated the pendant -OH groups on the surface of CDs to a carboxyl terminated chain transfer agent called 2-methyl-2-[(dodecyl sulfanylthiocarbonyl)sulfanyl]propanoic acid (C_{12} CTA) via Steglich esterification (figure 5.4). Water soluble luminous CDs/p (DMA) nano-composites were produced as a result of surface induced fragmentation chain transfer (RAFT) polymerization of N, N-dimethylacrylamide (DMA) from the surface of the CDs /C_{12} CTA[28].

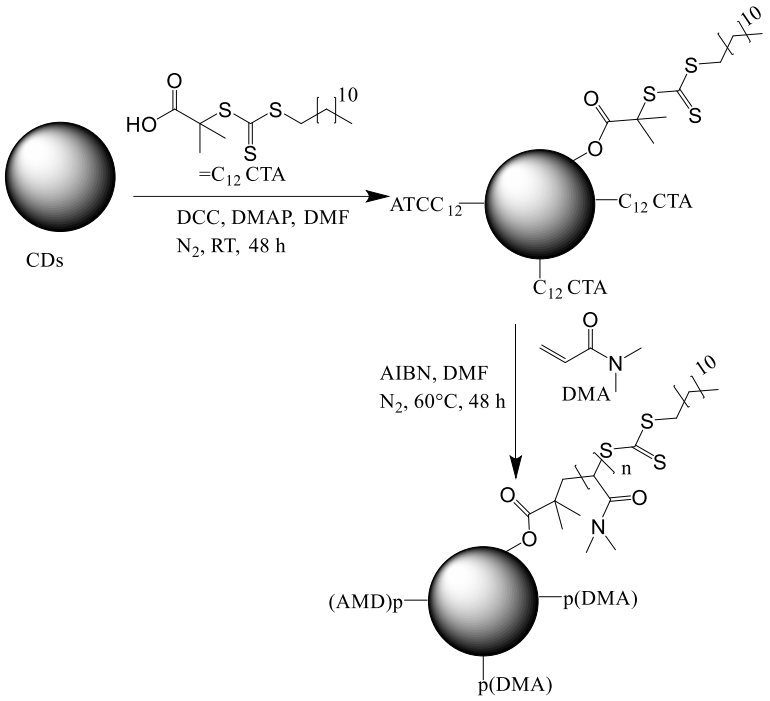

Figure 5.4. Reaction scheme for Steglich esterification between CDs and the C_{12} CTA and subsequent surface initiated RAFT polymerization of DMA[28].

Kaliyarson et. al. synthesized CDs from trimesic acid as precursor which is functionalized with amygdalin (natural chemotherapeutic agent) by a dehydration or esterification reaction. Through enzymatic hydrolysis by β-glucosidase, amygdalin separates into glucose molecules, benzaldehyde, and cyanide ions. In an acidic environment, the CDs were functionalized using amygdalin (Amy@CDs). Compared to normal cells, malignant neoplastic cells have a higher concentration of β-glucosidase. The Amy@CDs were used as the probe to determine the level of β-glucosidase. Their research suggests that the hybrid Amy@CDs may be useful for development of time-dependent anticancer therapies as well as the diagnostics of β-glucosidase in cancer cells[29].

CDs are a viable choice in the field of drug delivery because of their nontoxicity and nanocarrier qualities. As a nanocarrier for thymol, Murugesan et al. produced CDs; CDs–thymol conjugation was made by using a one-step esterification procedure. Briefly, they mixed the CDs and thymol in H_2SO_4 and refluxed the mixture for three hours at 110 °C. Diethyl ether was used to separate the generated conjugated ester extract. They proved that the arthritic activity of CDs-thymol is more effective than the standard drug ibuprofen[30].

In the extension of the application of CDs in the field of drug delivery Fahmi et al. showed how bamboo leaf cellulose might be used as a starting point for the formation of CDs for

imaging and drug delivery. 4-carboxybenzylboronic acid (CBBA) was added to the CDs using the Steglich catalyst. This catalyst was utilised to facilitate the esterification of the alcohol groups on the CDs and the carboxylic acid groups in the CBBA. Modified carbon dots enhanced the target selectivity of doxorubicin to HeLa carcinoma cells[31].

Another study also described the use of CDs for drug delivery and cellular uptake. Citric acid served as the carbon precursor and PEG diamine served as the capping agent in the synthesis of CDs by Krishna et al. Additionally, they synthesized conjugates by Stegleich esterification from CDs and DG (digitonin) at room temperature by using DCC/DMAP. Further they conjugated the methotrexate with CDs (CDMTX) to CDDG conjugate via esterification. The CDMTX combination demonstrated how DG affects the ability of drug carrier to be cytotoxic and increase cellular absorption. According to the study, CDs can be wisely modified to produce theranostic probes with enhanced properties[32].

In this work we are synthesizing the carbon dots from freshly prepared lemon juice. Most of the surface of carbon dots is covered by carboxylic groups on which Steglich esterification[33] reaction can take place with the curcuminoids by using N, N′-dicyclohexylcarbodiimide (DCC), and 4-dimethylaminopyridine (DMAP) as coupling agent. It has been reported that the ester bond can break in the acidic condition[34], so the developed nano architecture can play as pH triggered drug delivery system.

5.2. Experimental Section

5.2.1. Materials and methods

The chemicals and solvents used in the preparation of LCDs were of analytical grade. They were purchased from Sigma-Aldrich, Merck and used without further purification. FT-IR studies of all compounds were performed on Bruker Alpha FT-IR spectrometer in solid state as KBr pellets. NMR data was recorded on Bruker AVANCE, 400 MHz spectrometer in $CDCl_3$ and DMSO-d_6, with TMS as internal standard.

5.2.2. Synthesis of LCDs

Hydrothermal technology was used to make LCDs, as per the literature procedure[35]. In a 100 ml hydrothermal autoclave, 50 ml of filtered fresh lemon juice was added and held at 180 °C for 8 hours (scheme 5.1). The reaction was allowed to reach the room temperature after the completion and filtered using whatman paper. With the help of n-butanol, the LCDs were extracted from the filtrate. The extracted organic layer was dried using molecular sieves and concentrated under vacuum. The black sticky product was obtained and used directly in the next step.

Quantum Yield: 8.9 %

Zeta Potential (mV): -18.1

Z Size (d.nm): 648.3

IR (KBr disc, cm^{-1}): 3411.73(ν_{-O-H}), 1713.15($\nu_{-C=O}$), 1641.94($\nu_{-C=C}$), 1401.57(ν_{-C-H}), 1218.56(ν_{-C-O}).

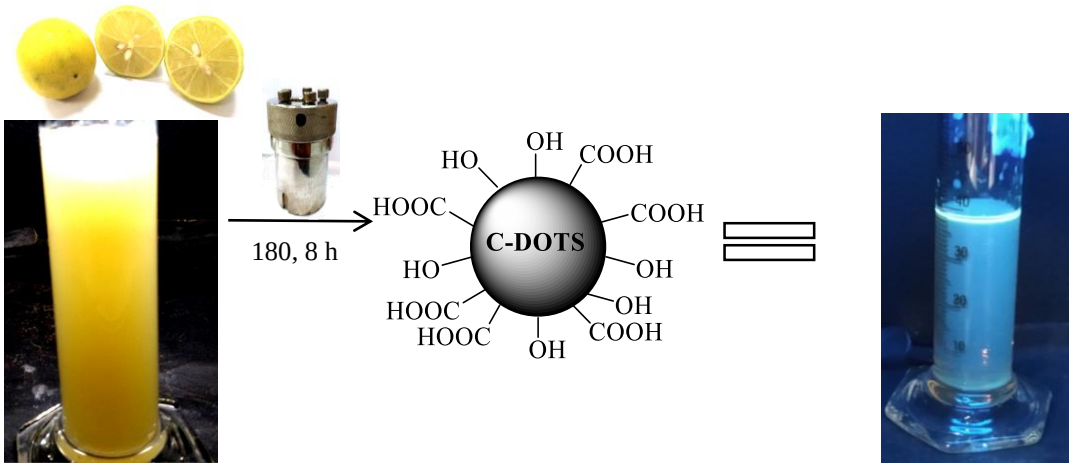

Scheme. 5.1. Synthesis of lemon derived carbon dots (LCDs) by Hydrothermal Method.

5.2.3. General method of Fabrication of LCDs

Dichloromethane was used to dissolve the dark sticky mass of previously synthesized LCDs. In a solution of LCDs, bis-demethoxy curcumin or curcuminoids (0.0016 moles), N, N′-dicyclohexylcarbodiimide (DCC) (0.0017 moles), and 4-dimethylaminopyridine (DMAP) (0.00016 moles) was added. The reaction mixture was stirred using magnetic stirrer at 30 ℃ for 24 hours. The reaction was filtered and the filtrate was washed with a 100 ml of saturated sodium chloride solution. The layer of dichloromethane was dried over sodium sulphate and completely evaporated using a rotary evaporator. The sticky yellowish brown substance was collected and purified further using dichloromethane:methanol :: 99:1 coloumn chromatography (scheme 5.2).

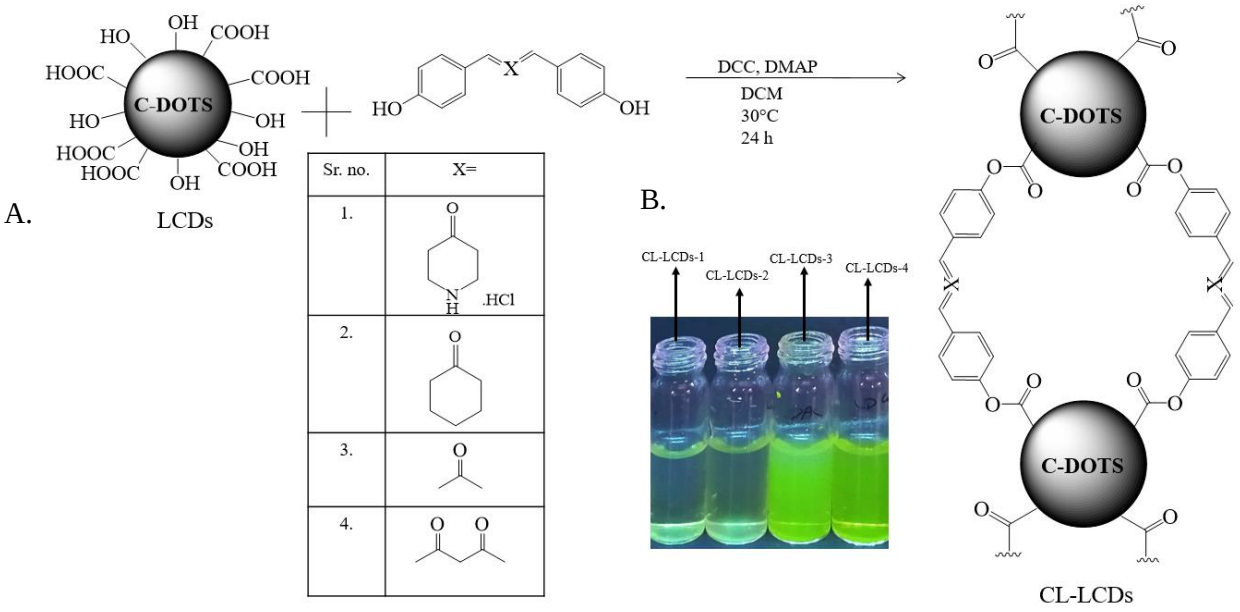

Scheme 5.2. A.) Synthesis of curcuminoid linked lemon carbon dots (CL-LCDs) by esterification reaction. B.) Fluorescence of different CL-LCDs.

5.2.3.1. Synthesis of CL-LCDs-1

0.5 g [0.0016 moles] 3,5-bis((E)-4-hydroxybenzylidene)piperidin-4-one was added to the solution of LCDs in dichloromethane and stirred for 10 min. 0.368 g [0.0017 moles] dicyclohexylcarbodiimide (DCC) and 0.0198 g [0.00016 moles] DMAP were added into the reaction according to the general procedure 5.2.3. Product was purified using silica gel column chromatography with dichloromethane:methanol solvent (scheme 5.3).

Z Size (d.nm): 389.6

Zeta Potential (mV): -18.7

IR (KBr disc, cm^{-1}): 1730.82 ($\nu_{-C=O,}$ ester), 1192.86($\nu_{-C-O-C,}$ ester).

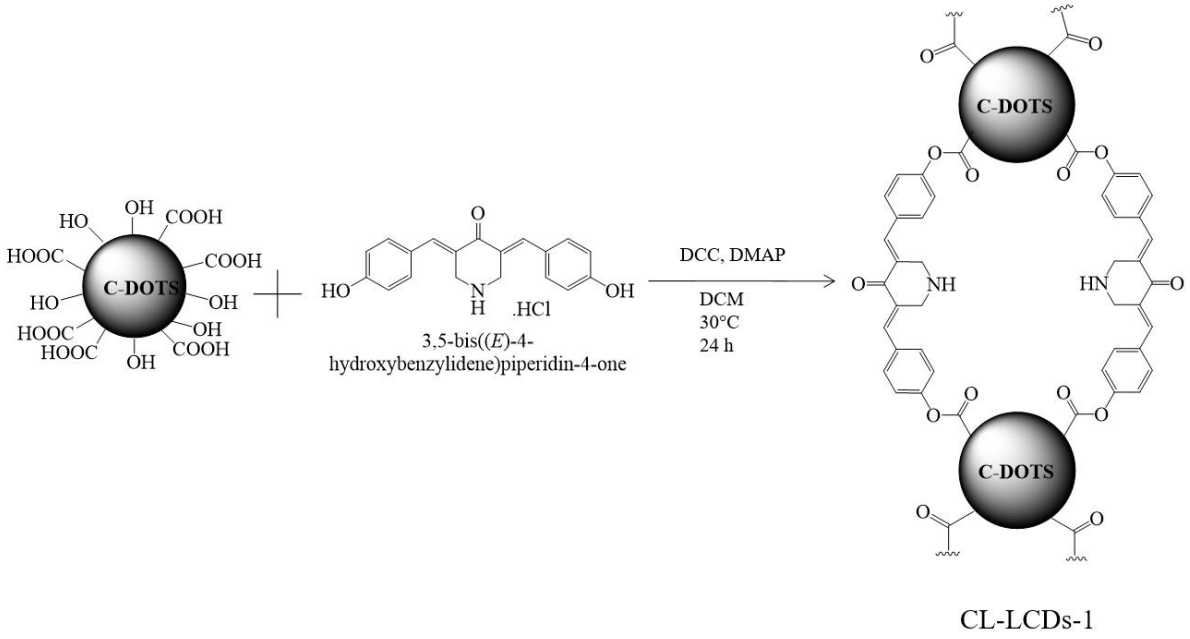

CL-LCDs-1

Scheme. 5.3. Synthesis of piperidone based curcuminoid linked lemon carbon dots (CL-LCDs-1) by esterification reaction.

5.2.3.2. Synthesis of CL-LCDs-2

0.5 g [0.0016 moles] 2,6-bis((E)-4-hydroxybenzylidene)cyclohexan-1-one was added to the solution of LCDs in dichloromethane and stirred for 10 min. 0.368 g [0.0017 moles] dicyclohexylcarbodiimide (DCC) and 0.0198 g [0.00016 moles] DMAP were added into the reaction according to the general procedure 5.2.3. Product was purified using silica gel column chromatography with dichloromethane:methanol solvent (scheme 5.4).

Z Size (d.nm): 233.3

Zeta Potential (mV): -10.6

IR (KBr disc, cm^{-1}): 1700.23($\nu_{-C=O,}$ ester), 1243.30($\nu_{-C-O-C,}$ ester).

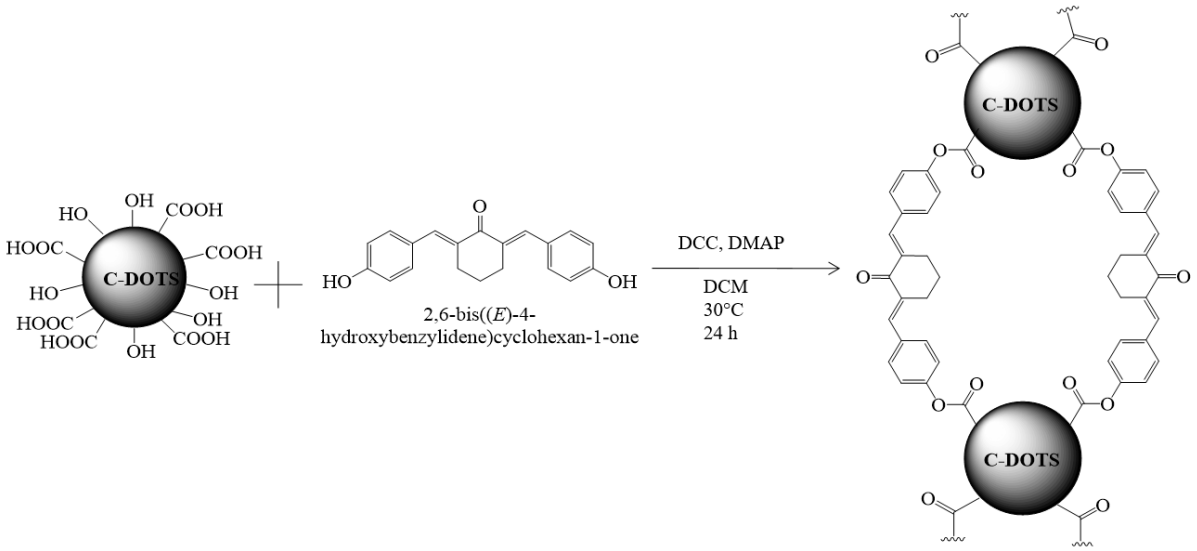

CL-LCDs-2

Scheme. 5.4. Synthesis of cyclohexanone based curcuminoid linked lemon carbon dots (CL-LCDs-2) by esterification reaction.

5.2.3.3. Synthesis of CL-LCDs-3

0.5 g [0.0018 moles] (1E,4E)-1,5-bis(4-hydroxyphenyl)penta-1,4-dien-3-one was added to the solution of LCDs in dichloromethane and stirred for 10 min. 0.426 g [0.0020 moles] dicyclohexylcarbodiimide (DCC) and 0.0229 g [0.00018 moles] DMAP were added into the reaction according to the general procedure 5.2.3. Product was purified using silica gel column chromatography with dichloromethane:methanol solvent (scheme 5.5).

Z Size (d.nm): 243

Zeta Potential (mV): -14.1

IR (KBr disc, cm^{-1}): 1734.33($\nu_{-C=O,}$ ester), 1167.51($\nu_{-C-O-C,}$ ester).

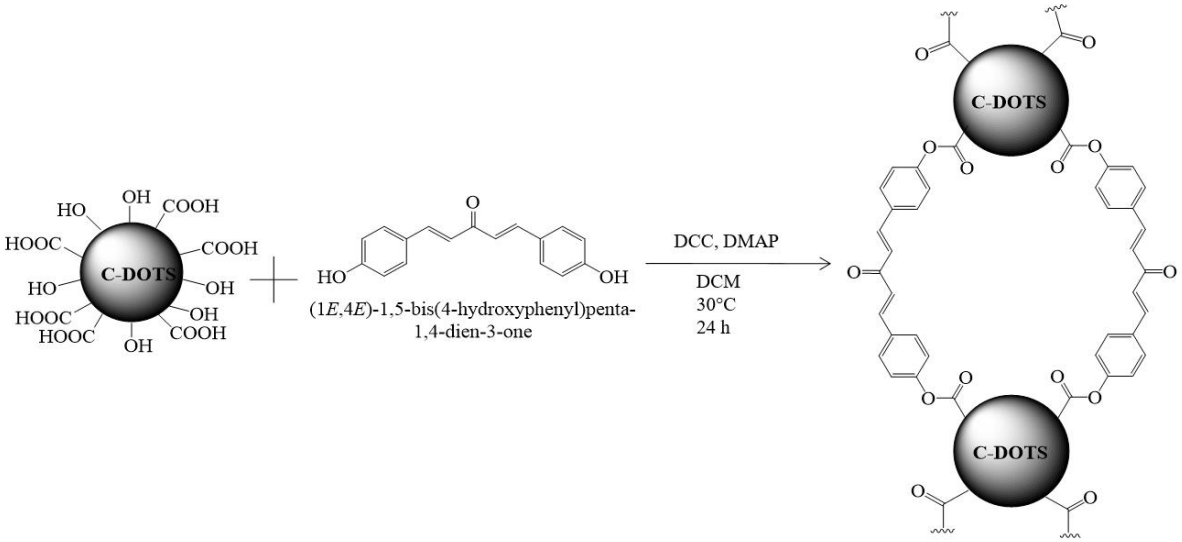

CL-LCDs-3

Scheme. 5.5. Synthesis of acetone based curcuminoid linked lemon carbon dots (CL-LCDs-3) by esterification reaction.

5.2.3.4. Synthesis of CL-LCDs-4

0.5 g [0.0016 moles] bisdemethoxycurcumin was added to the solution of LCDs in dichloromethane and stirred for 10 min. 0.368 g [0.0017 moles] dicyclohexylcarbodiimide (DCC) and 0.0198 g [0.00016 moles] DMAP were added to the above solution and the reaction was continued according to the general procedure 5.2.3. Product was purified using silica gel column chromatography with dichloromethane:methanol::99:1 solvent (scheme 5.6).

Z Size (d.nm): 205.5

Zeta Potential (mV): -38.4

IR (KBr disc, cm^{-1}): 1735.16 ($\nu_{-C=O,}$ ester), 1168.58($\nu_{-C-O-C,}$ ester).

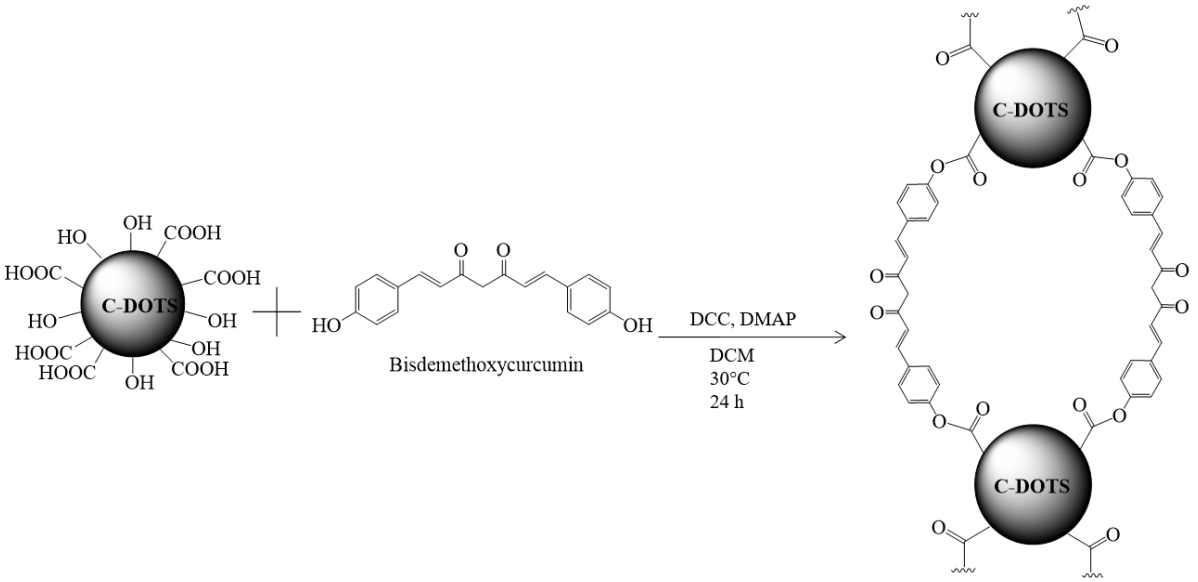

CL-LCDs-4

Scheme. 5.6. Synthesis of bisdemethoxy curcumin linked lemon carbon dots (CL-LCDs-4) by esterification reaction.

5.2.4. Quantum Yield Measurement

The solution of quinine sulphate in 0.1 M H_2SO_4 (QY = 0.546) was chosen as a reference. Comparing integrated photoluminescence intensity (excited at 300 nm) and absorbance (less than 0.1 at 300 nm) of each samples to those of quinine sulphate, allowed to determine the QY of LCDs. The following equation was used to determine the QY of LCDs[36].

$$\varphi_x = \varphi_{st} (I_x/I_{st}) (A_{st}/A_{x)} (\eta_x/\eta_{st})^2$$

where,

Φ = the quantum yield,
I = fluorescence intensity,
A = absorbance at excitation wavelength
η = solvent's refractive index.
The subscript ‘st’ denotes standard whose quantum yield is known, while ‘x’ denotes the sample.

5.2.5. Inclusion of Drug

Drug methotrexate (MTX) was encapsulated by kneading method. 1 mg of CL-LCDs and 10 mg of MTX with few drops of dichloromethane, ethanol and water was kneaded. It was allowed to air dry for few days at room temperature. Free flowing powder was obtained.

5.2.6. Calculation of Drug Loading (DL%) of CL-LCDs and Encapsulation Efficiency (EE%) of Methotrexate

2 ml of the 2 mg/ml MTX ⊂ CL-LCDs aqueous solution was dialysed using a dialysis bag (MWCO: 500 da) in 100 ml of aqueous medium at 37 °C to calculate the drug loading and encapsulation efficiency. Utilising an ultraviolet detection wavelength of 300 nm, spectrophotometry was used to quantify the amount of MTX contained in the inclusion complexes. Using the following formulae, the drug loading (DL) and entrapment efficiency (EE) were estimated in comparison to the standard curve:

$$DL\ (\%) = [(W_{MTX} - W_{Unbound\ MTX}) / W_{Inclusion\ complex})] \times 100$$

$$EE\ (\%) = [(W_{MTX} - W_{Unbound\ MTX}) / W_{MTX})] \times 100$$

Where,

W_{MTX} = Weight of MTX in inclusion complex

$W_{Unbound\ MTX}$ = Weight of unbound MTX released from inclusion complex

$W_{Inclusion\ complex}$ = Weight of inclusion complex[37]

5.2.7. Cumulative release of Methotrexate

2 ml aqueous solution of 2 mg/ml MTX ⊂ CL-LCDs was dialysed using a 0.1-0.5 kD MWCO, Float-A-Lyzer G2, CE, Dialysis Membrane device from Repligen (Spectrum Laboratories), Inc. in 100 ml of the buffer solution at 37°C. The study was carried out with PBS (Phosphate buffer solution) of pH 7.4 and PBS of pH 5.5. PBS of pH 7.4 mimics the normal physiological medium and PBS with pH 5.5 simulates the tumour microenvironment. To determine the cumulative drug release, the UV-Vis spectrometer was used to quantify the dialysate at 300 nm during the drug release.

5.2.8. Cytotoxicity Assay

The MTT colorimetric assay was performed to evaluate the in vitro cytotoxic activity of MTX ⊂ CL-LCDs against cervical cancer cell line HeLa and normal human embryonic kidney cell line HEK-293. Firstly, both cell lines were maintained under appropriate condition environment. HeLa and HEK-293 cells were harvested in minimum essential medium (MEM) supplemented with 10% Fetal Bovine Serum (FBS) and maintained at 37°C supplemented with 100 I. U./ml Penicillin-Streptomycin, 5 % CO_2 in a CO_2 incubator (Remi, India) with 95% humidity. The cell lines obtained from each log-phase of growth were harvested by trypsinization and then resuspended in complete growth medium to give a total of 2×10^4 cells/ml. Then, 200 µl of the cell suspension was seeded into the wells of 96-well plates (Tarson). The plates were incubated overnight in a humidified air atmosphere at 37°C with 5% CO_2. After overnight incubation, the cells were treated with the compounds in concentration range of 0.01-100 µg/ml. The plates were incubated for further 24 h. At the highest concentration of the compounds applied, DMSO accounted for 0.2% of the final concentration. In each plate three control wells (cells without test compounds) and blank wells (the medium with 0.2% DMSO) were kept for cell viability determination. After completion of 24 h incubation time, 10 µl MTT (5 mg/ml), was added to each wells, followed by 4 h of incubation. After incubation, in each well, the culture medium was then replaced with 100 µl of DMSO. After 30 min incubation the plate was shaken for 1 min and then using a microplate reader (Analabs), the absorbance of each well was measured by at 490 nm. For each compound, the concentration that inhibits 50% cell growth has been determined (IC_{50}).

5.3. Results and Discussion

The pH triggered sustained release drug delivery system could be designed by developing the architectures from carbon dots which are linked by curcuminoids. By choosing the natural product based precursors such as Lemon juice and curcumin derivatives (Curcuminoids) we developed MTX loaded curcuminoid linked LCDs which are well tolerated by normal cells. Curcumin and lemon are part of daily meal of Asian community. Due to their biofunctional qualities, such as their anti-tumour, antioxidant, and anti-inflammatory actions, curcumin and its derivatives have attracted a great deal of research over the past 20 years[38].

By selecting specific precursors with medicinal properties during synthesis, functionalization, and surface passivation, properties of the CDs can be continuously updated and altered. In this work we are synthesizing the carbon dots from freshly prepared lemon juice.

Citric acid (48 mg/ml), ascorbic acid (47 mg/ml), and maleic acid (2.3 mg/ml) are the principal carbon-containing components of lemon juice[39]. LCDs were created using the hydrothermal process over the course of 8 hours at 180 °C using 50 ml of fresh lemon juice (scheme 5.1). Currently, the potential mechanisms for the hydrothermal technique of producing LCDs from carbon precursors have been put out and studied[40]. According to the literature, the filtered lemon juice when subjected to hydrothermal reaction create the core C=C/C-C skeleton of LCDs. The remaining molecules then approach the surface of the core to create new C-C/ C=C bonds, which are subsequently continually developed in the same manner[41]. The morphology of LCDs gradually takes shape when heating time is extended. The edge and surface of LCDs may consists of a significant amount of carboxyl (-COOH), hydroxyl (-OH), carbonyl (-C=O), or other oxygen-containing functional groups as a result of the hydrothermal treatment process that created them. As seen in scheme 1, the creation of LCDs from fresh lemon juice resulted in the change of its colour from ivory-white to a dark brown. Under the UV lamp, the LCDs glow intensely blue (scheme 5.1).

Architectures from the LCDs were further achieved by use of DCC and DMAP which activate the carboxylic acid groups present on the surface of LCDs.

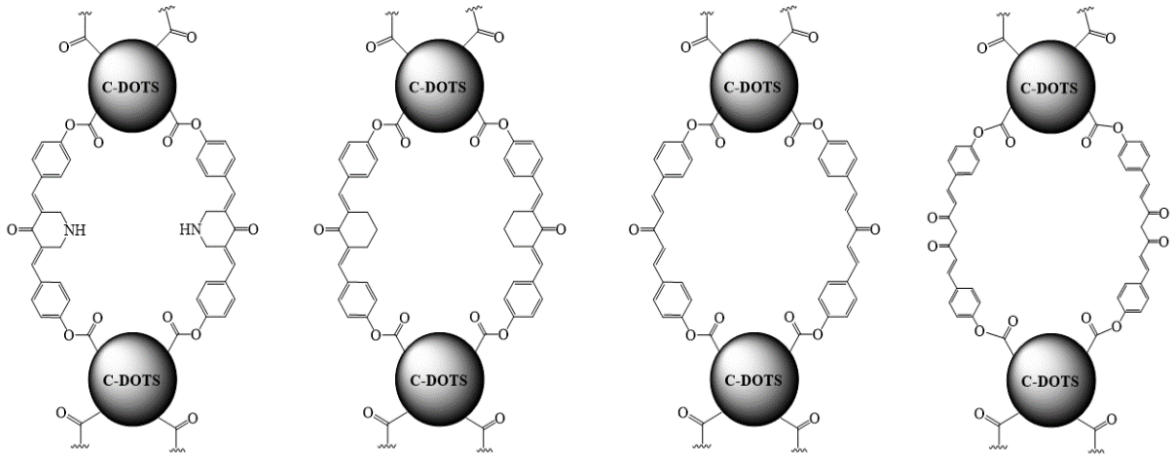

Figure.5.5. Curcuminoid linked lemon carbon dots (CL-LCDs).

The activated carboxylic acid group undergoes esterification and get covalently linked with the curcumin and curcuminoids (figure 5.5). Column chromatography was used to purify the produced curcuminoid linked lemon carbon dots (CL-LCDs). The synthesized LCDs and CL-LCDs are characterized by various techniques such as UV- Vis, Fluorescence, FT-IR, NMR, DLS, SEM and HR-TEM.

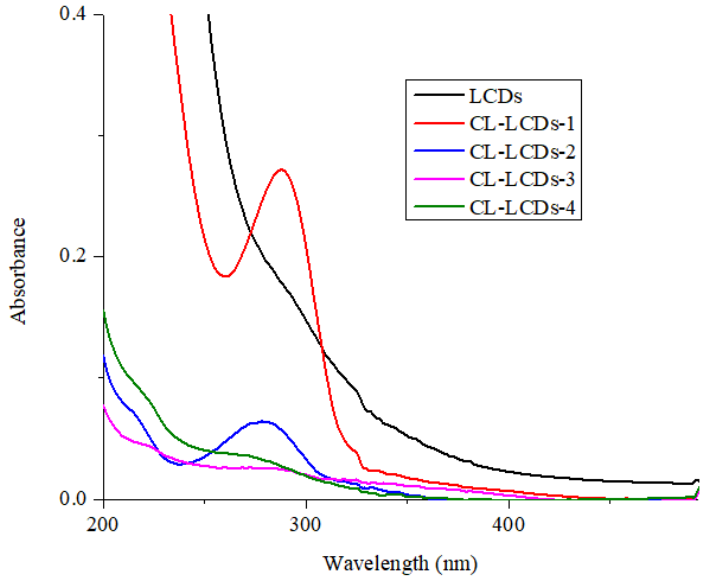

Figure. 5.6. UV-Vis absorption spectra of lemon derived carbon dots (LCDs) and curcuminoid linked lemon carbon dots (CL-LCDs).

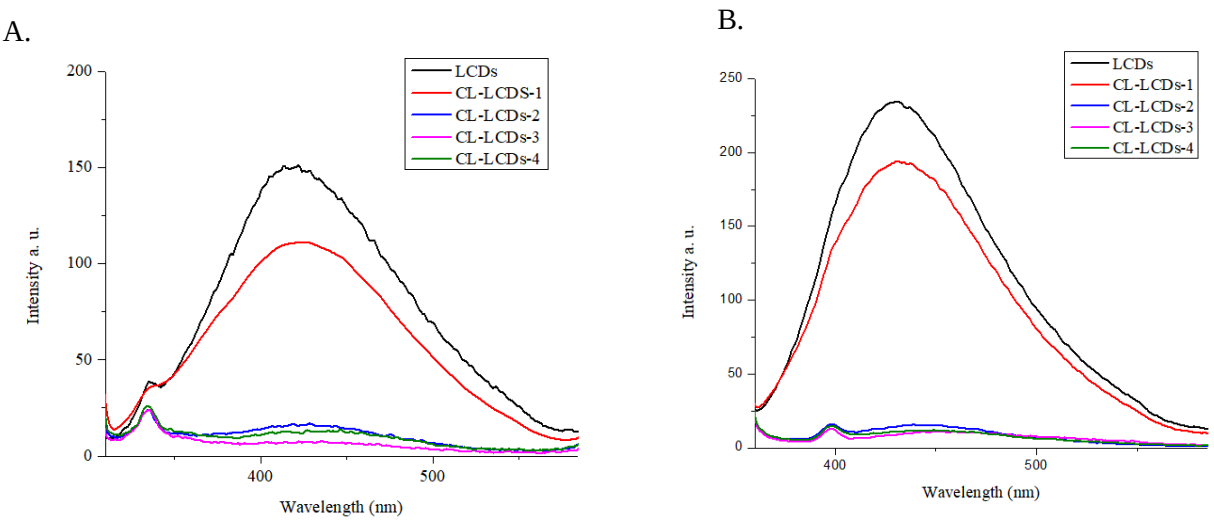

Figure. 5.7. PL (Photoluminescence) spectra of LCDs and CL-LCDs, A.) Excitation at 300 nm, B.) Excitation at 350 nm.

The photoluminescence (PL) and ultraviolet-visible (UV-Vis) absorption spectra of LCDs were measured to investigate the optical characteristics of LCDs. As illustrated in (Figure. 5.6), the optical absorption peak of LCDs was discovered to be in the ultraviolet region, with an absorption maximum at 283 nm and a tail extending into the visible range due to the n-π* transition of the C=O group[42]. According to the PL spectrum in figure. 5.6, PL emission wavelength peaks of LCDs at 417 nm with an excitation wavelength of 300 nm (figure 5.7 A) and at 429 nm with an excitation wavelength of 350 nm were observed (figure 5.7 B). The excitation wavelength was changed from 300 to 350 nm, which resulted in a shift of the emission wavelength from 417 to 429 nm. The red shift of fluorescence emission peak on selecting the higher excitation wavelength, indicates the photon reabsorption. It also reveals that the PL property of LCDs is excitation-dependent[43]. Additionally, the quantum-confinement effect and edge defects are associated with a broad photoluminescence peak that moves with the change in excitation wavelength in the fluorescent LCDs[41]. The fluorescence quantum yield of the LCDs using the conventional PL measurement[44], where quinine sulphate had been utilised as the reference, is 8.9% at an excitation wavelength of 300 nm.

The PL emission wavelength of LCDs moved to a longer wavelength and the intensity dropped slightly after the esterification on its surface with piperidone based curcuminoid (figure. 5.7), while fluorescence of LCDs got quenched drastically in the case of other derivatives of LCDs. This result shows that among all the derivatives of LCDs only CL-LCDs-1 derivative can be used for the bio-imaging application.

The FT-IR spectrum of LCDs is displayed in spectrum 5.1. Peaks at 3411.73 cm^{-1} (O-H stretching vibrations), 2982.37 cm^{-1}, 2937.62 cm^{-1}, 2607.51 cm^{-1}, 1401.57 cm^{-1} (C-H stretching vibrations), 1713.50 cm^{-1} (C=O stretching vibrations), 1641.94cm^{-1} (C=C stretching vibrations), and 1218.56 cm^{-1} (C-O stretching vibrations), cm^{-1} suggested the existence of oxygen containing functionalities in LCDs.

The esterification onto the surface of LCDs was also confirmed by comparing their FTIR spectrum. In case of architectures, the C=O band at 1713 cm^{-1} of carboxylic acid group vanishes. A distinct band at 1735.16 cm^{-1} due to C=O stretch and a strong band at 1168.58 cm^{-1} due to C–O-C stretch signify the presence of ester groups on the surface of the CL-LCDs-4 (spectrum 5.5). Esterification of acetone-based curcuminoid on surfaces of LCDs to achieve CL-LCDs-3 results in significant stretching vibration due to the ester C=O group at 1734.33 cm^{-1} and C-O-C group at 1167.51 cm^{-1} (spectrum 5.4).

When curcuminoids based on cyclohexanone moiety are connected onto LCDs surfaces to achieve CL-LCDs-2, the ester group exhibits marked C=O stretching at 1700.23 cm^{-1} as well as C-O-C stretching at 1243.30 cm^{-1} (spectrum 5.3). Similarly, in the case of piperidone-based curcuminoid CL-LCDs-1, the ester group is identified by significant C=O stretch at 1730.82 cm^{-1} and C-O-C stretch at 1192.85 cm^{-1} after being linked to the surface of LCDs (spectrum 5.2).

Furthermore, the distinction between sp^3- and sp^2 -hybridized carbon atoms was made using nuclear magnetic resonance (NMR) spectroscopy of LCDs. The ^1H NMR spectrum of LCDs shown in spectrum 5.6 shows the four distinct regions listed below each include a distinctive chemical environment. The ^1H NMR spectrum (spectrum 5.6) was found to contain the following chemical shift regions: 1-3 ppm protons attached to sp^3 hybridized carbon), 3-6 ppm (protons of hydroxyl, and ether groups), 6-8 ppm (protons attached to sp^2 hybridized carbon of aromatic ring), and a broad singlet at 9.398 ppm. The NMR reveals that carbon atoms that have undergone sp^3 and sp^2 hybridization are present in carbon quantum dots.

The synthesis of architectures is further supported by ^1H NMR spectra. There is a distinct change in ^1HNMR spectra after esterification reaction, where peak at 9.398 ppm is vanished in CL-LCDs (spectrum 5.7-5.10) and other peaks are shifted downfield.

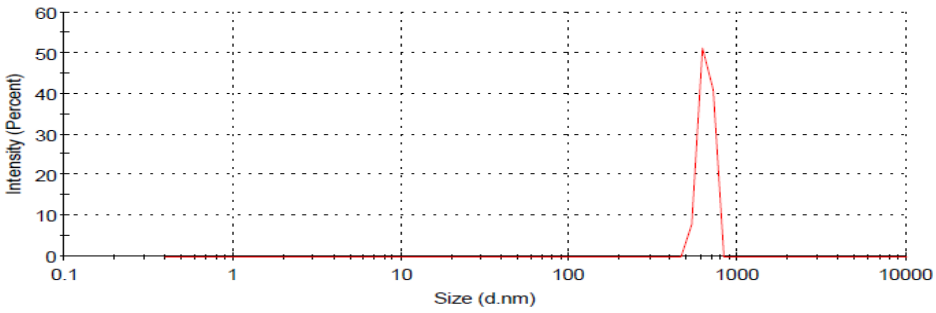

Figure. 5.8. DLS measurement of LCDs.

The hydrodynamic diameter of the synthesised LCDs, as seen in figure 5.8, is approximately 648.3 nm. The acquired zeta potential measurement of LCDs is found to be -18.1 mV, which indicates the surface charge due to the presence of –COOH and –OH on the surface of LCDs. FEG-SEM, and HR-TEM techniques were used to describe size and morphology of LCDs.

A.

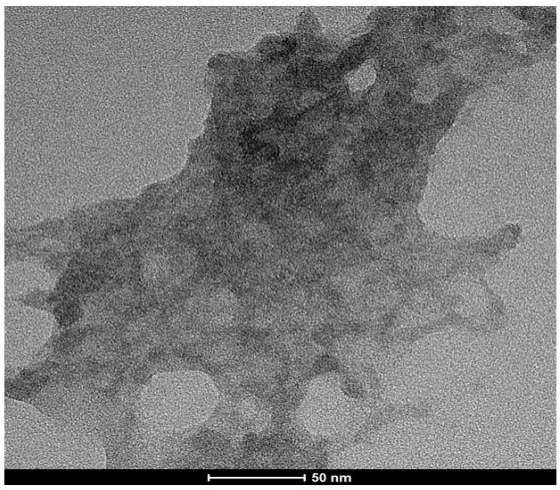

B.

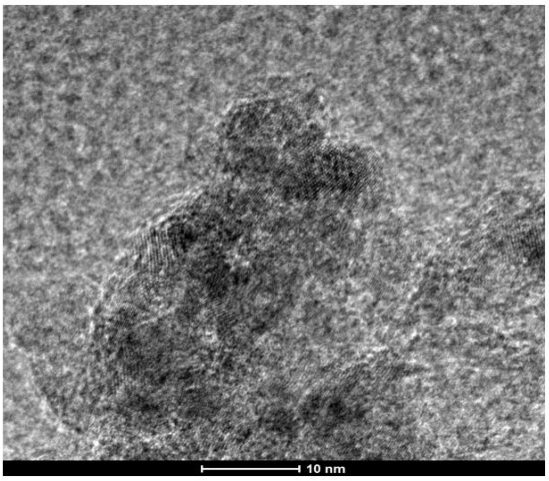

Figure. 5.9. HR-TEM images of lemon derived carbon dots (LCDs): (A Scale bar 50 nm (B. Scale bar 10 nm.

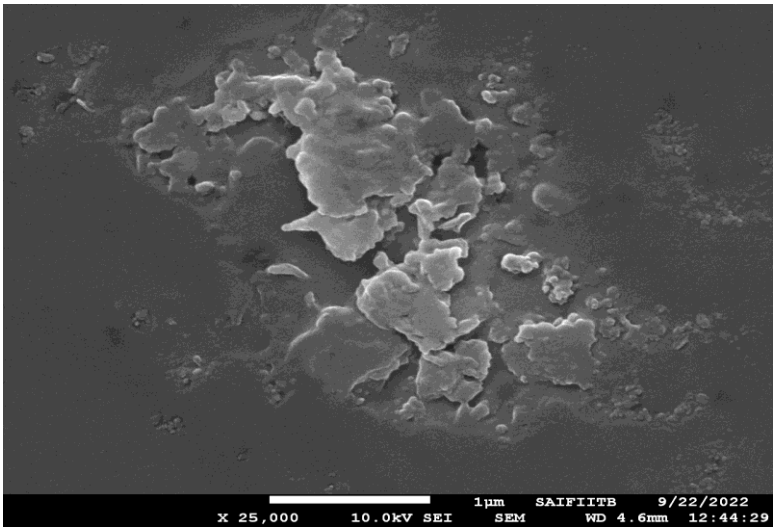

Figure. 5.10. FEG-SEM images of LCDs scale bar at 1 µm.

The LCDs have a size range of 10 to 12 nm as revealed from HR-TEM images (figure 5.9) and seem spherical and evenly distributed in FEG-SEM images (figure 5.10). After the synthesis of architectures from LCDs, the hydrodynamic diameter decreases due to the increment of the hydrophobicity of the system. The hydrodynamic diameter of CL-LCDs-4 is 205.5 nm and its zeta potential is -38.4 mV (figure 5.11 D). In case of CL-LCDs-3, with an acetone derived curcuminoid linker, the hydrodynamic diameter is 243 nm and zeta potential is -14.1mV (figure 5.11 C).

On the other hand, increment of hydrophobicity with alicyclic linker in case of cylohexanone based curcuminoid CL-LCDs-2 the hydrodynamic diameter decreases up to 233.3 nm and zeta potential is -10.6 mV (figure 5.11 B). On the attachment of relatively polar of piperidone derived linker on the surface of LCDs to achieve CL-LCDs-1, the hydrodynamic diameter increases up to 389.6 nm and zeta potential is found to be -18.7 mV (figure 5.11 A).

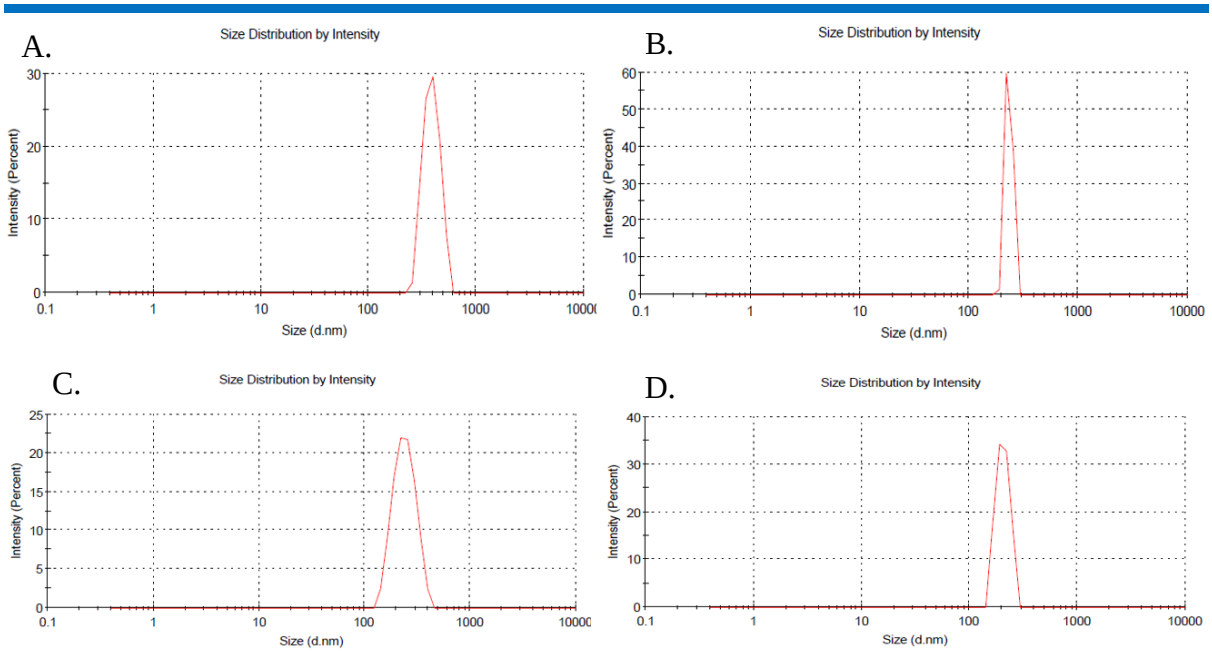

Figure. 5.11. DLS of curcuminoid linked lemon derived carbon dots (CL-LCDs). A.) CL-LCDs-1, B.) CL-LCDs-2, C.) CL-LCDs-3, D.) CL-LCDs-4.

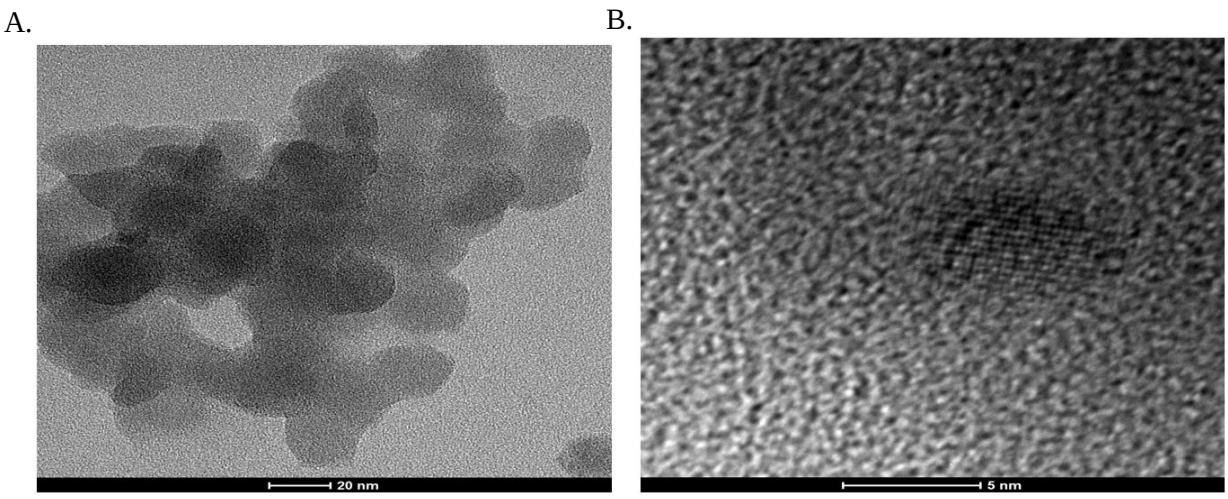

Figure. 5.12. HR-TEM images of CL-LCDs-4 A. at 20 nm, C. at 5 nm.

Using HR-TEM, the morphology of CL-LCDs-4 was examined. As shown in figure 5.12, the formation of cross-linked nano-architectures of CL-LCDs-4, resulted in the size distribution of 10 nm to 5 nm from HR-TEM images. The nanostructure of CL-LCDs-4 reveals the lattice spacing of 0.37 nm. The size of CL-LCDs-4 derivative falls within the range of preferred sizes for development of efficient drug delivery system[45].

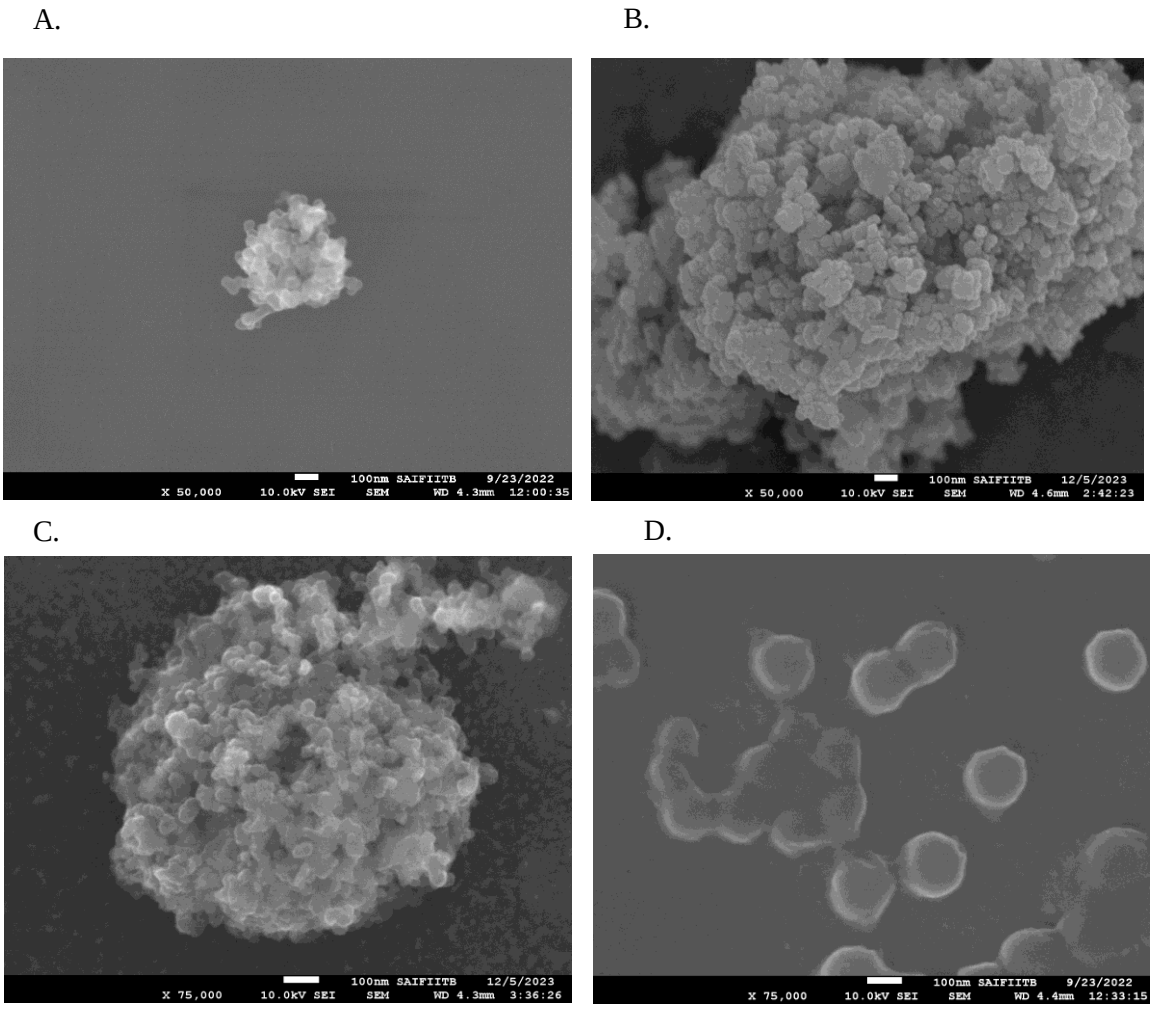

Figure. 5.13. FEG-SEM images of A. CL-LCDs-1 at 100 nm, B. CL-LCDs-2 at 100 nm, C. CL-LCDs-3 at 100 nm, D. CL-LCDs-4 at 100 nm.

The morphologies of the prepared CL-LCDs, was revealed from FEG-SEM images (figure 5.13). The homogeneity in the shape and size was further demonstrated by SEM pictures.

The size distribution obtained from the DLS approach is bigger than the particle size obtained from the HR-TEM, because CL-LCDs-4 aggregates and go through a swelling process in aqueous media[46].

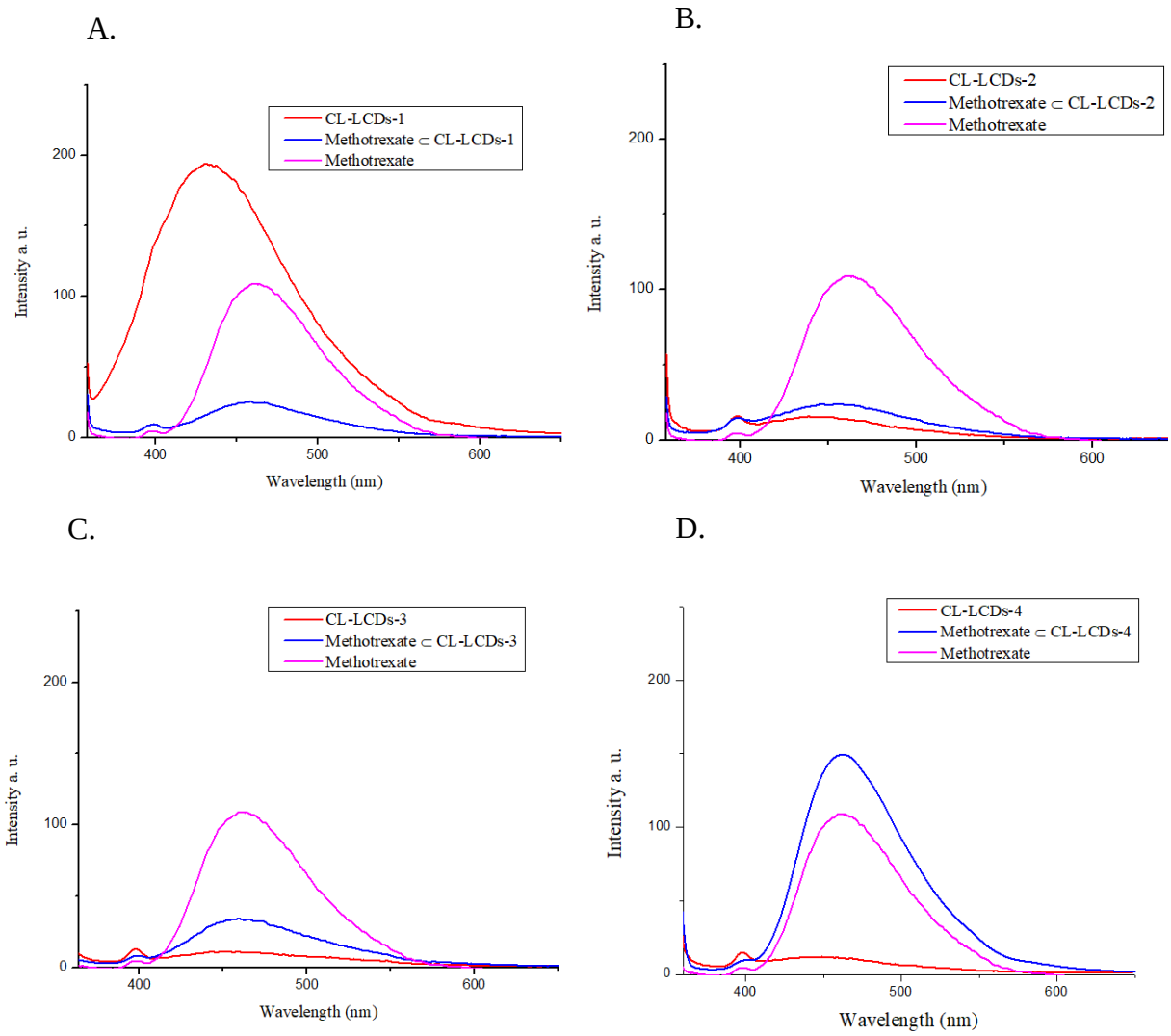

Figure. 5.14. PL spectra of curcuminoid linked lemon derived carbon dots (CL-LCDs), MTX loaded CL-LCDs and MTX. A) PL spectra of CL-LCDs-1, MTX loaded CL-LCDs-1 and MTX, B) PL spectra of CL-LCDs-2, MTX loaded CL-LCDs-2 and MTX, C) PL spectra of CL-LCDs-3 MTX loaded CL-LCDs-3 and MTX, D) PL spectra of CL-LCDs-4, MTX loaded CL-LCDs-4 and MTX.

Methotrexate was selected to be the drug delivered using the synthesized CL-LCDs as a nanocarrier. The anticancer and anti-inflammatory drug methotrexate (MTX) is frequently used to treat autoimmune illnesses and many forms of cancer. Although MTX has a limited role in cancer treatment due to its drug resistance, narrow therapeutic index, poor absorption, and low water solubility, these factors are dose-dependent[47]. To overcome this problem MTX was loaded in CL-LCDs nanoarchitectures by kneading method to enhance drug transport to the intended tissue, lessen MTX cytotoxicity, and boost its effectiveness. MTX has two

carboxylic acid and amine group in its structure which can form hydrogen bond with the ester and ketone group of CL-LCDs. The binding of MTX can also be supported through π-π stacking with the aromatic rings of CL-LCDs. The FT-IR spectra of MTX loaded CL-LCDs showed the change in absorption band compare to their parent molecule (spectrum 5.11).

The PL emission spectra of MTX loaded CL-LCDs derivatives shows that among all the derviatives of CL-LCDs only CL-LCD-4 enhances the fluorescence of MTX while other derivatives CL-LCD-2 and CL-LCD-3 quenches the fluorescence of drug while CL-LCDs-1 quenches fluorescence of MTX as well as itself (figure 5.14). This result suggested that CL-LCD-4 can be used as to track the pathway of drug loaded CL-LCDs-4 while CL-LCD-1 can be used to investigate the excretion pathway of its own.

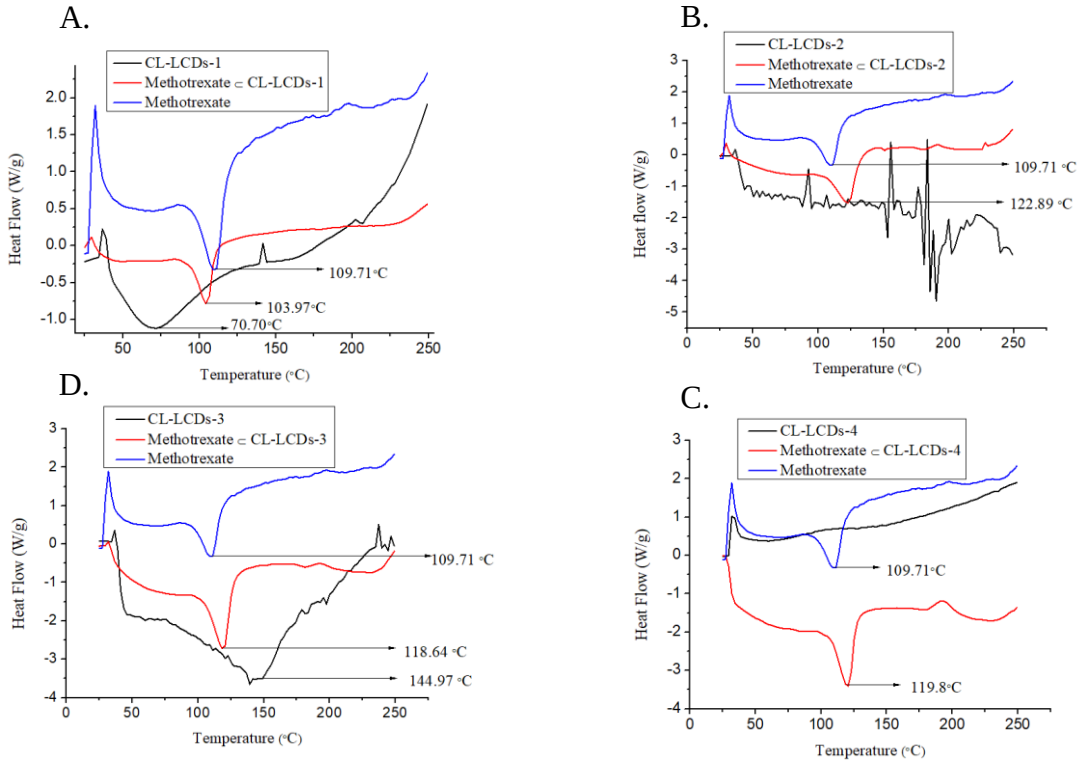

Figure. 5.15. DSC thermogram of curcuminoid linked lemon derived carbon dots (CL-LCDs), MTX loaded CL-LCDs and MTX. A) CL-LCDs-1, MTX loaded CL-LCDs-1 and MTX, B) CL-LCDs-2, MTX loaded CL-LCDs-2 and MTX, C) CL-LCDs-3, MTX loaded CL-LCDs-3 and MTX, D) CL-LCDs-4, MTX loaded CL-LCDs-4 and MTX.

DSC is a useful tool to determine how many phases are present in systems[48]. It is also effective for determining how well a drug interacts with its carrier[49,50]. As a result, the thermal behaviour of MTX, CL-LCDs, and MTX encapsulated CL-LCDs were investigated using DSC to

characterise the potential for complexation and/or any potential interactions. (Figure 5.15) The DSC thermogram for MTX alone revealed one distinctive abrupt endothermic peak at about 109.71 °C, which is related to its melting temperature[51] (figure 5.15). The DSC thermograms showed that the strength of the endothermic melting point peak of MTX was greatly reduced and shifted to a higher temperature after the encapsulation into CL-LCDs-4 (figure 5.15 D), CL-LCDs-3 (figure 5.15 C), and CL-LCDs-2 (figure 5.15 B), at about 119.8 °C, 118.64 °C and 122.89 °C respectively. The endothermic melting point peak of MTX, however, was moved to a lower temperature at about 103.97°C in the case of a CL-LCDs-1 (figure 5.15 A). These alterations in the endothermic peak of MTX indicated that MTX well interacted with CL-LCDs and got encapsulated.

Sr. no	Inclusion complex	EE%	DL%
1.	MTX ⊂ CL-LCDs-1	62.59 %	56.90 %
2.	MTX ⊂ CL-LCDs-2	56.36 %	46.88 %
3.	MTX ⊂ CL-LCDs-3	92.17 %	83.66 %
4.	MTX ⊂ CL-LCDs-4	74.97 %	68.15 %

Table. 5.1. Encapsulation efficiency MTX and Drug loading capacity of methotrexate loaded curcuminoid linked lemon derived carbon dots (MTX ⊂ CL-LCDs).

CL-LCDs-1 (Table 5.1) showed 56.90 % drug loading, 62.59 % encapsulation efficiency and CL-LCDs-2 (Table 5.1) showed 46.88 % drug loading, 56.36 % encapsulation efficiency. A highest drug loading capacity (83.66 %) and encapsulation efficiency (92.17 %) was attained in case of CL-LCDs-3 (Table 5.1). CL-LCDs-4 (Table 5.1) showed 68.15 % drug loading and 74.97 % encapsulation efficiency. The high drug loading capacity of CL-LCDs-3 and CL-LCDs-4 may be attributed to flexible nature of the monoketone and β-diketone based curcumnoid linker which can change the voids in order to accommodate more methotrexate molecules. The other factors which affect the drug loading are as follows. The distinctive central hollow cavity structure of CL-LCDs could offer plenty of room for drug storage; second, the non-covalent bonding between CL-LCDs and MTX was also advantageous for drug loading; and third, the large cavity between CL-LCDs created by the linking of curcumin analogues.

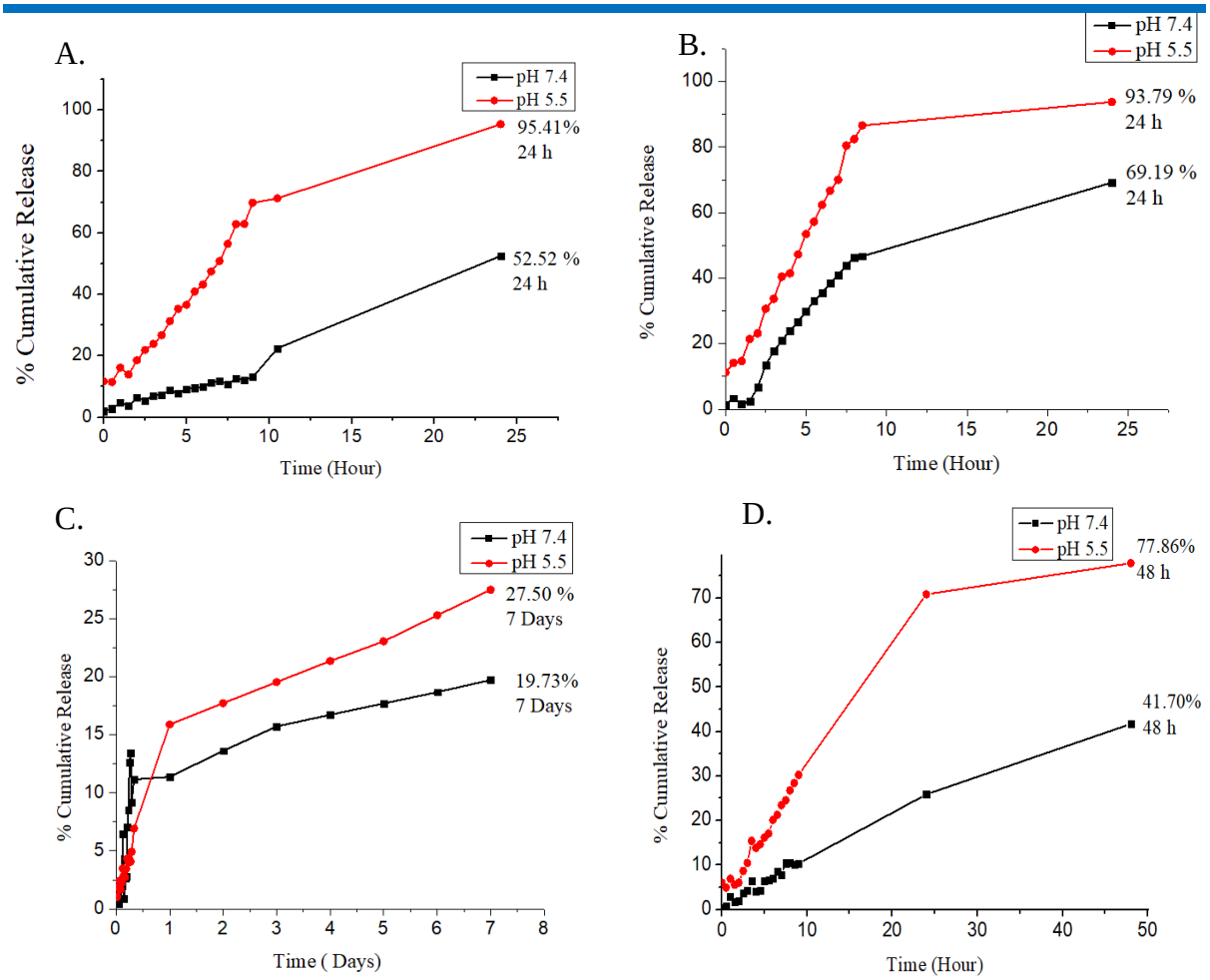

Figure. 5.16. Cumulative release of MTX from the MTX loaded curcuminoid linked lemon derived carbon dots (MTX ⊂ CL-LCDs) A) MTX ⊂CL-LCDs-1, B) MTX ⊂CL-LCDs-2, C) MTX ⊂CL-LCDs-3, D) MTX ⊂CL-LCDs-4 .

In any of the release profiles, there were no discernible burst release. CL-LCDs-1 and CL-LCDs-2 (figure 5.16 A, B) showed the comparable cumulative release of 95.41 % and 93.79 % in 24 hours at pH 5.5. In the instance of CL-LCDs-3 (figure 5.16 C), the release of drug was quick in the initial 24 h, with a total release of 15.12 %. After that, a steady, continuous drug release became apparent; by 7 days, a cumulative release of 27.50 % was attained. The sustained release of drug from CL-LCDs-3 might be due to compact structure formed between the drug and CL-LCDs-3. Minimal drug release is anticipated to reduce the harmful effects of MTX on healthy cells and tissues. The sustained drug release was also observed in case of CL-LCDs-4 (figure 5.16 D). 70.85 % of drug was released in 48 hours at pH 5.5. The two factors that should be responsible for the slow controlled drug release are: (i) the slow diffusion of the drug MTX which was released out of the CL-LCDs and (ii) the re-absorption of the released MTX by the CL-LCDs.

Sr. No	Inclusion complex	IC_{50} HeLa (µg/ml)	IC_{50} HEK 293 (µg/ml)
1	CL-LCDs-1	50.07 ± 25.031	45.8 ± 1.0
2	CL-LCDs-2	1327 ± 475.32	49.91 ± 1.56
3	CL-LCDs-3	10.81 ± 10.3	55.59 ± 3.2
4	CL-LCDs-4	14.36 ± 9.49	80.39 ± 0.67
5	MTX ⊂ CL-LCDs -1	0.00818 ± 0.008781	37.02 ± 1.2
6	MTX ⊂ CL-LCDs -2	0.01425 ± 0.012729	25.19 ± 0.56
7	MTX ⊂ CL-LCDs -3	1.411 ± 1.599399	80.28 ± 2.3
8	MTX ⊂ CL-LCDs -4	0.01512 ± 0.017722	51.69 ± 0.45
9	MTX	94.19 ± 5.485656	81.61 ± 3.6

Table. 5.2. Cytotoxicity of CL-LCDs, MTX ⊂ CL-LCDs, and MTX against HeLa and HEK 293 cancer cells for 24 hours incubation by MTT assay.

The cytotoxicity of MTX ⊂ CL-LCDs-1, MTX ⊂ CL-LCDs-2, MTX ⊂ CL-LCDs-3, MTX ⊂ CL-LCDs-4, and MTX was evaluated using the MTT cell viability assay on Hela and Hek293. The lowest inhibitory concentration IC_{50} (the concentration of the drug that inhibits 50% of the cell viability) was discovered after cells were treated with various receptor concentrations (1 to 100 M) for 24 hours (table 5.2). The observed IC_{50} values on HeLa cell line for MTX ⊂ CL-LCDs-1, MTX ⊂ CL-LCDs-2, MTX ⊂ CL-LCDs-3 and MTX ⊂ CL-LCDs-4 were 0.008181, 0.01425, 1.411, and 0.01512 µg/ml, respectively. The inclusion complexes show around 100 to 1000 times better IC_{50} values on HeLa cell line than free MTX.They are well tolerated by normal cells as revealed by IC_{50} values of HEK 293. While MTX ⊂ CL-LCDs-3 showed only a modest impact on the suppression of cancer cells, the MTX ⊂ CL-LCDs-4 and MTX ⊂ CL-LCDs-2 showed much better cytotoxicity. The MTX ⊂ CL-LCDs-1 exhibits best cytotoxic activity. This reveals that structural modification in CL-LCDs affects the cytotoxicity. As per prior art, the replacement of β-diketo moiety with cyclohexanone and piperidone[52] results in increased bioavailability and activity of curcumin, which is reflected in IC_{50} values of MTX ⊂ CL-LCDs-1 and MTX ⊂ CL-LCDs-2. The lower cytotoxicity of MTX ⊂ CL-LCDs-3 as compared to MTX ⊂ CL-LCDs-4 is might be due to slow release of MTX from the carrier which is reflected in its release profile.

5.4. Conclusion

We have developed four different curcuminoid linked LCDs from lemon juice using steglich esterification. The particle size of CL-LCDs-4 was found to be 10 nm as revealed by HR-TEM images which is preferred for development of drug delivery system. The anticancer drug MTX was loaded and preferentially released under pH stimuli. The highest drug loading and entrapment efficiency were found to be 83.66 % and 92.17 % with CL-LCDs-3. The CL-LCDs-3 was found to have most sustained release of MTX while CL-LCDs-4 was found to have adequate release profile with 70.87% release in 24 h. The MTX ⊂ CL-LCDs-3 exhibit poor cytotoxicity as compared to other formulations on HeLa cell line due to controlled release of MTX from CL-LCDs-3 while MTX ⊂ CL-LCDs-4 has better cytotoxicity with adequate release profile. The MTX ⊂ CL-LCDs-1 shows best cytotoxicity on HeLa cell line which can be attributed to the structural modification in the curcuminoid where piperidone moiety is introduced. The piperidone based CL-LCDs-1 might be better facilitating the cell internalization with 95% drug release in 24 hours

5.5 Analytical Data

Spectrum 5.1: FT-IR spectrum of LCDs

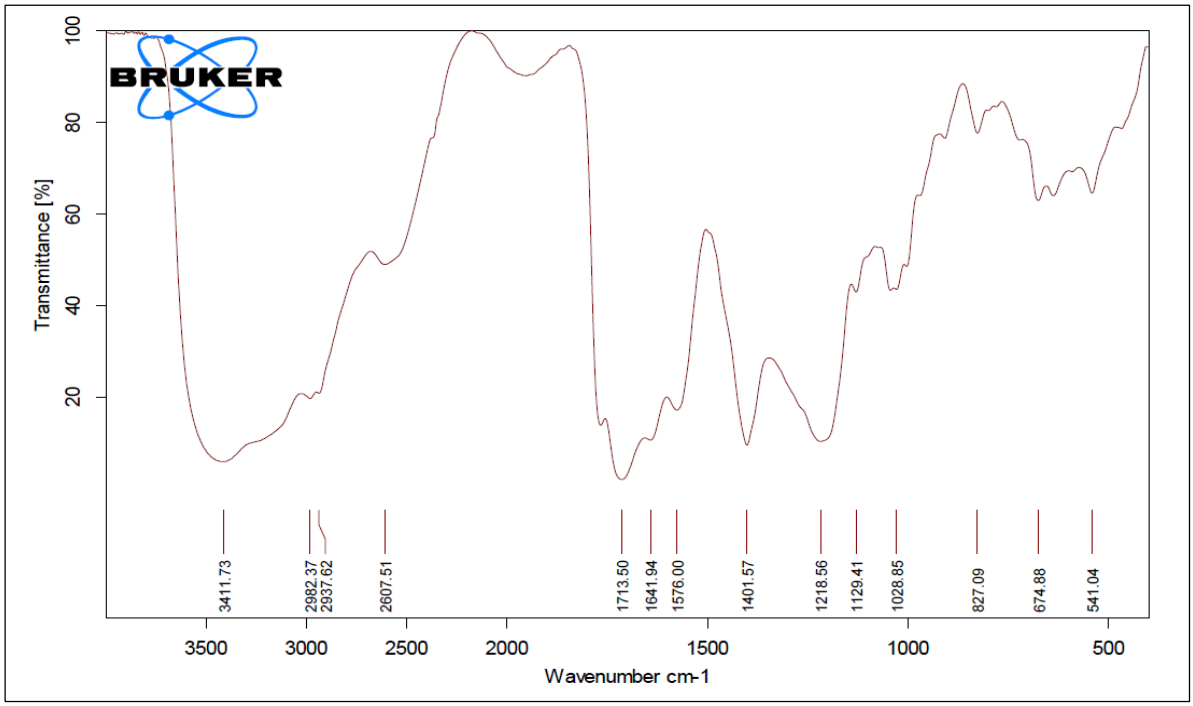

Spectrum 5.2: FT-IR spectrum of CL-LCDs-1

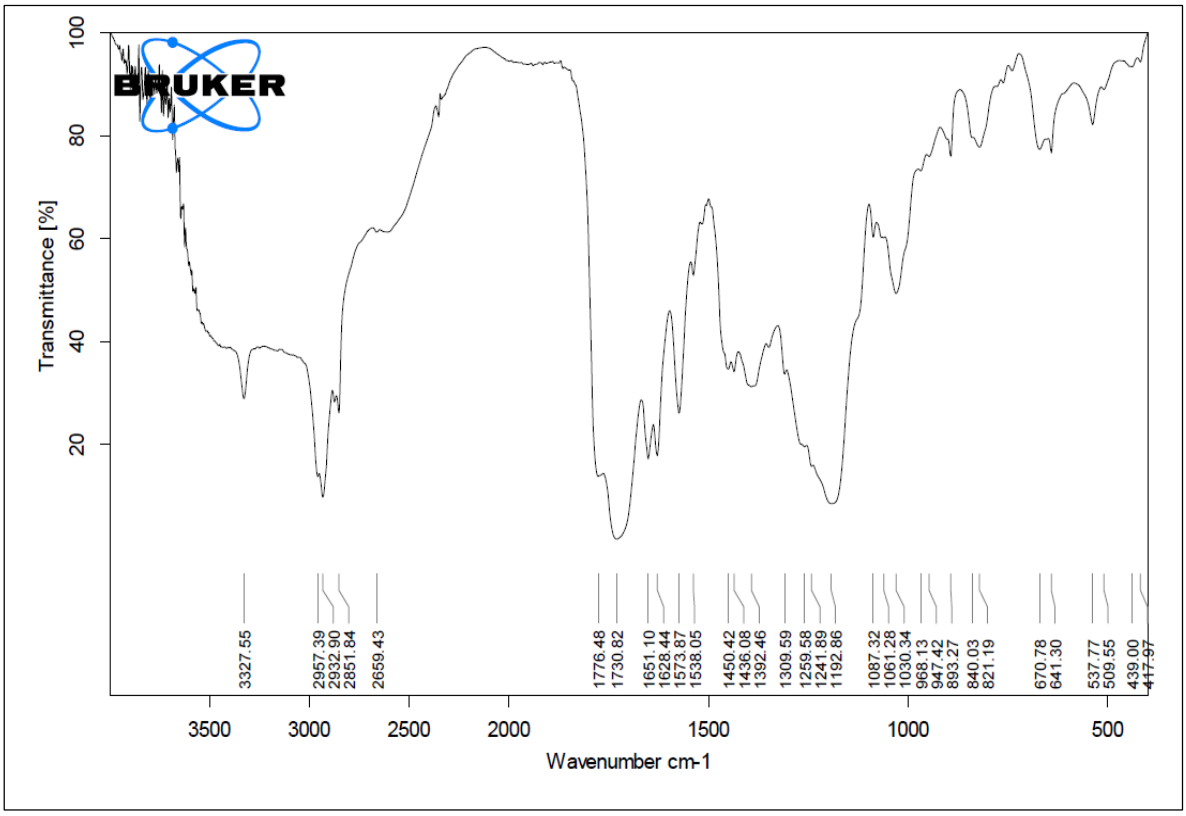

Spectrum 5.3: FT-IR spectrum of CL-LCDs-2

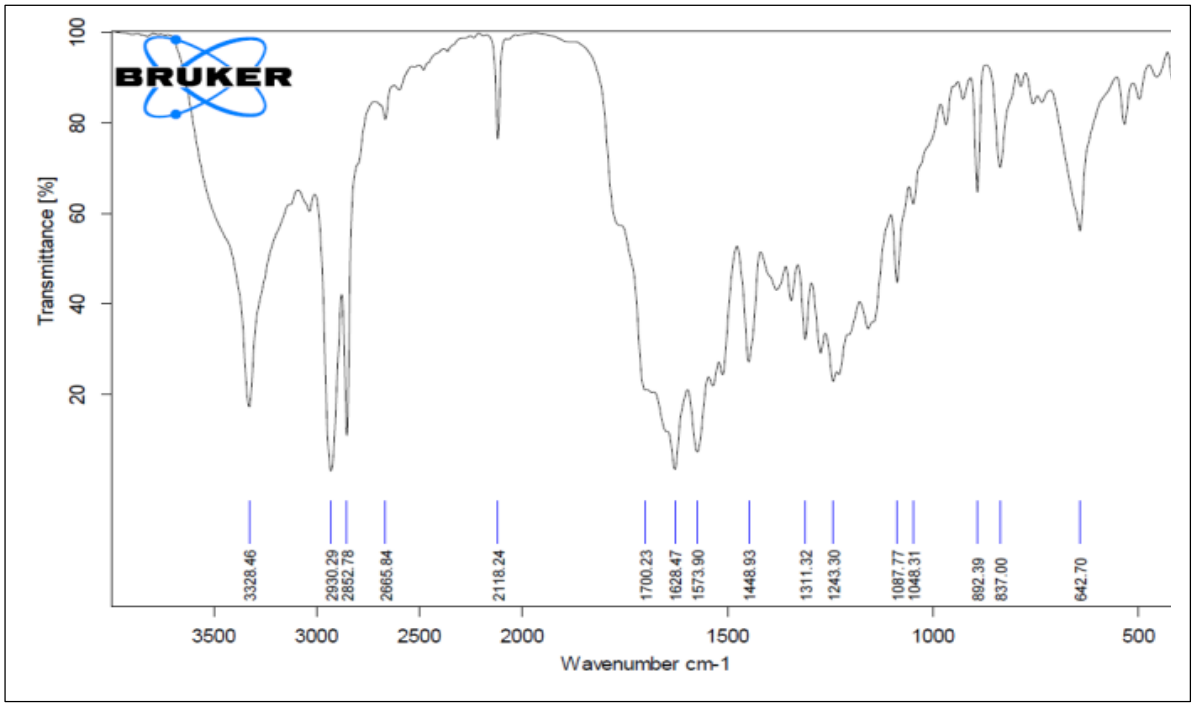

Spectrum 5.4: FT-IR spectrum of CL-LCDs-3

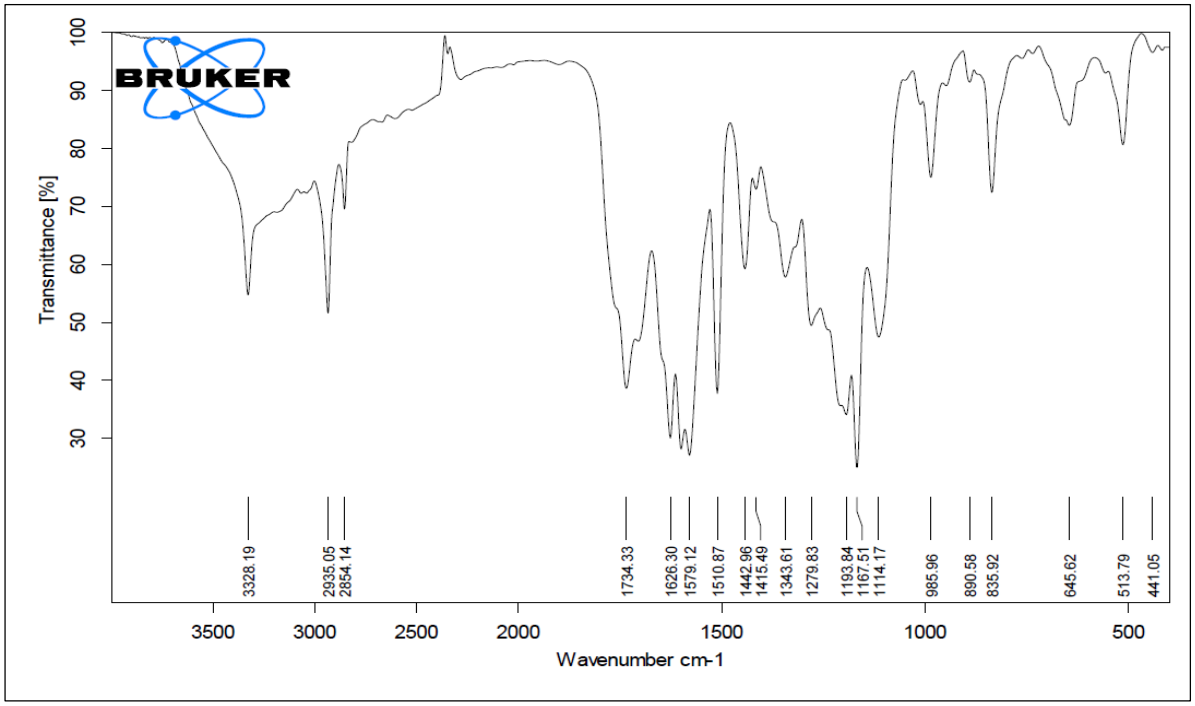

Spectrum 5.5: FT-IR sectrum of CL-LCDs-4

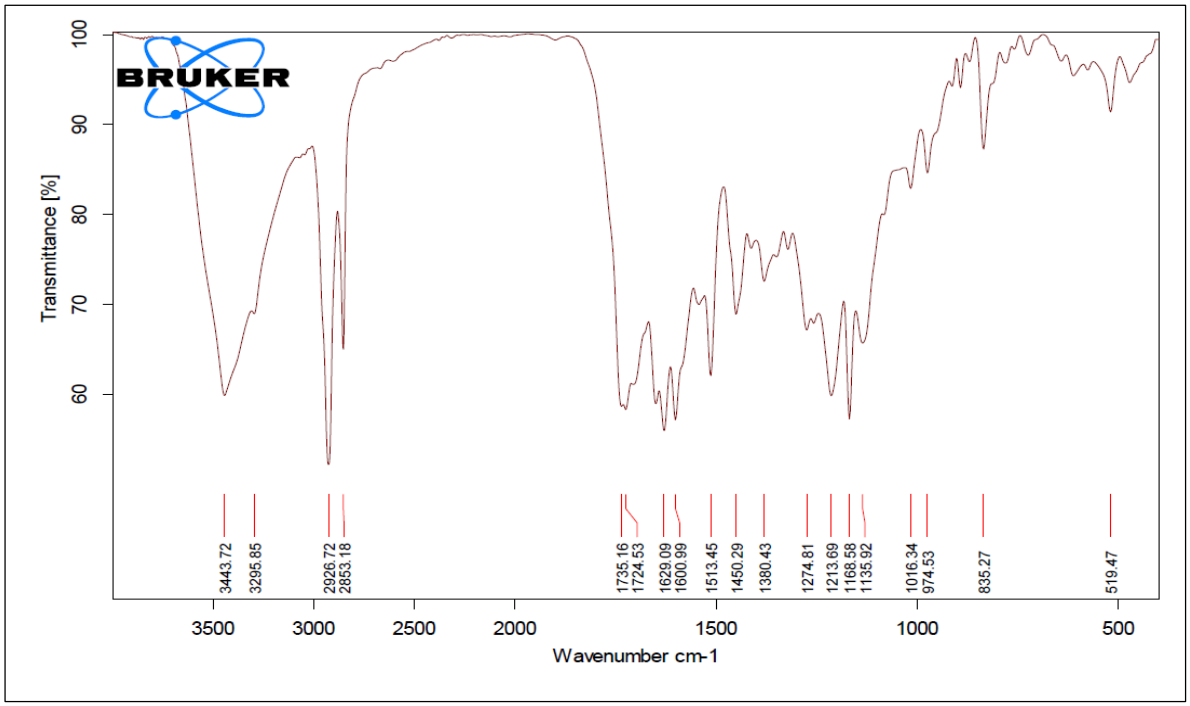

Spectrum 5.6: ^{1}H NMR spectrum of LCDs

DMSO-d_6

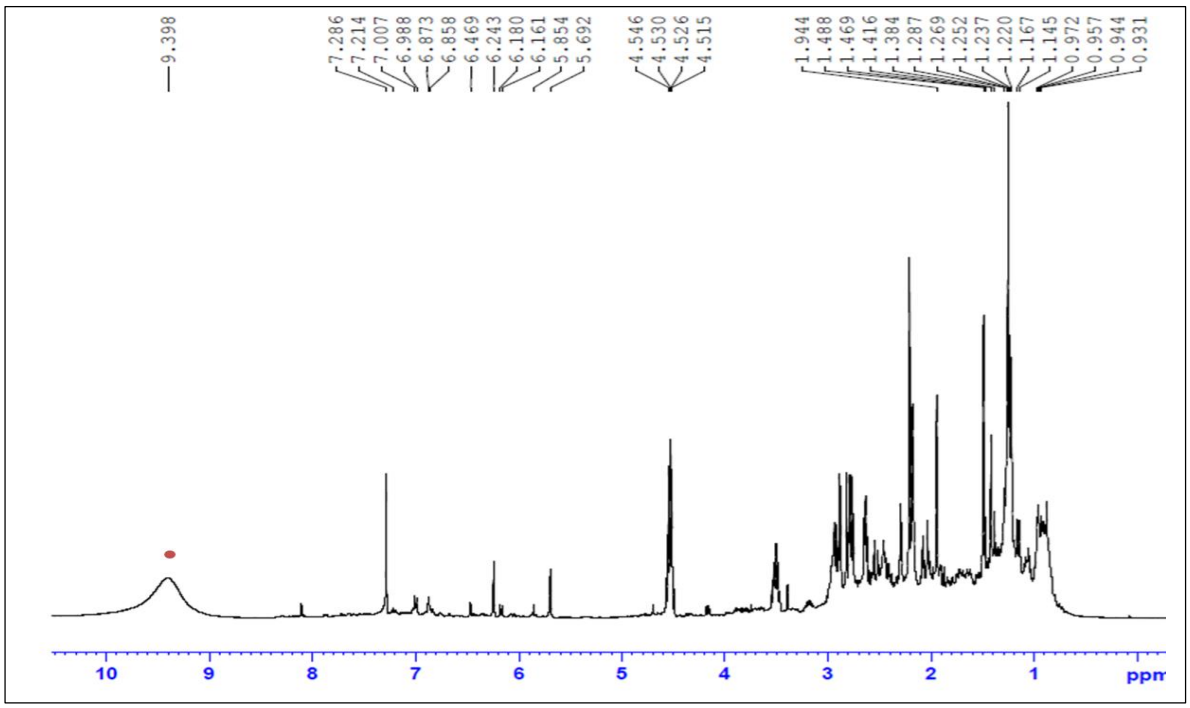

Spectrum 5.7: ^{1}H NMR spectrum of CL-LCDs-1 **DMSO-d_6**

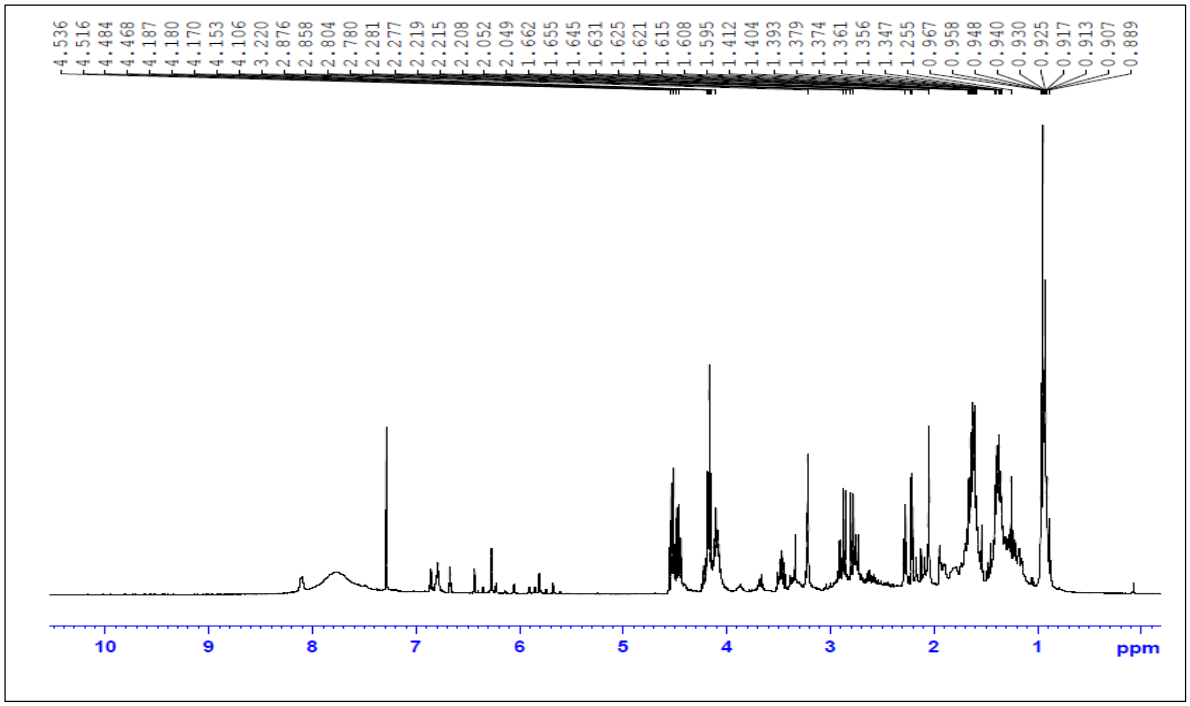

Spectrum 5.8: ^{1}H NMR spectrum of CL-LCDs-2

DMSO-d_6

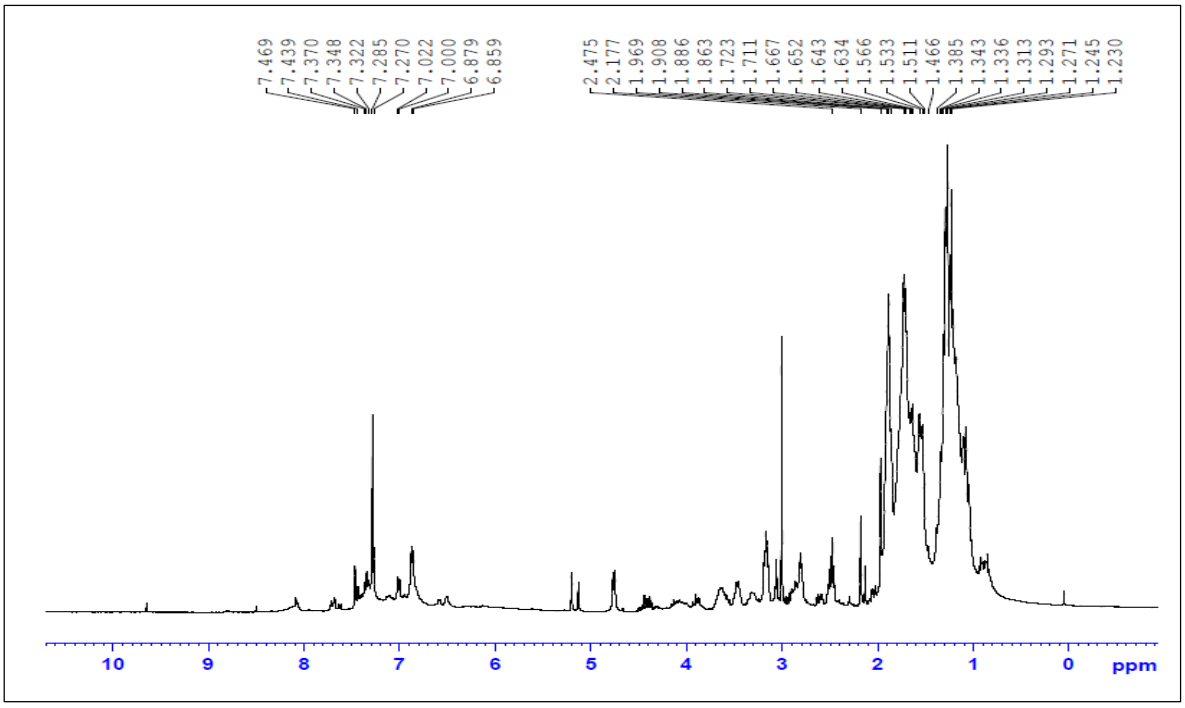

Spectrum 5.9: ^{1}H NMR spectrum of CL-LCDs-3 **DMSO-d_6**

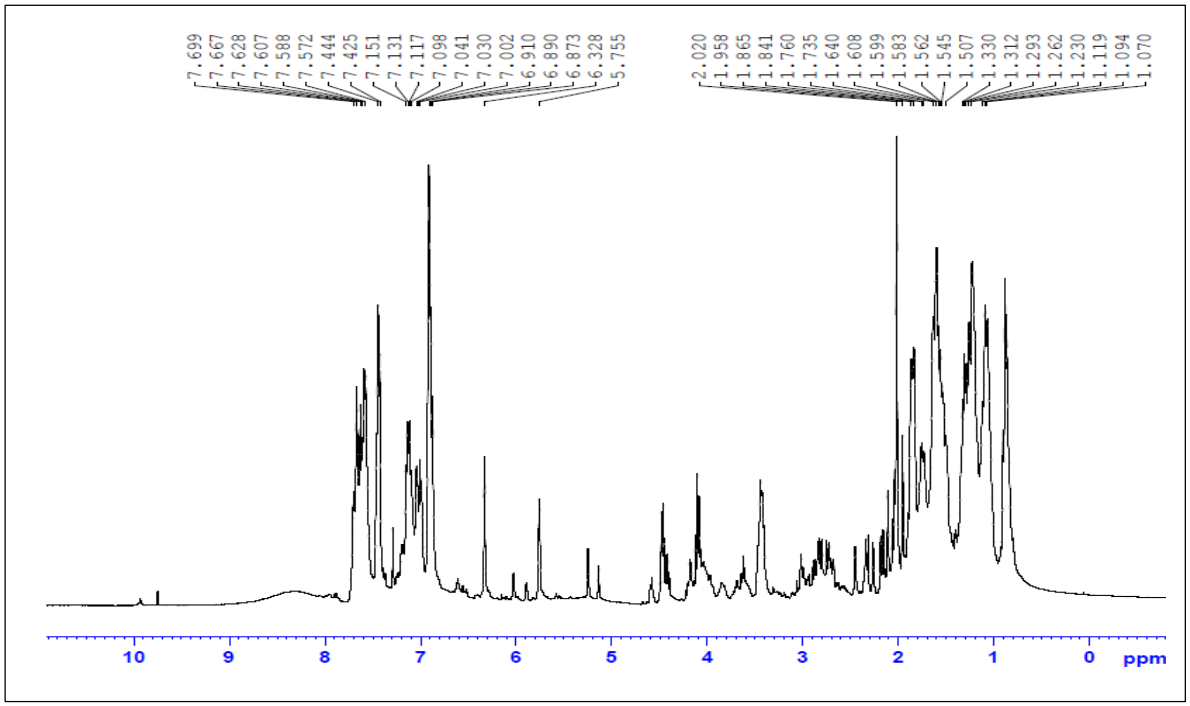

Spectrum 5.10: ^{1}H NMR spectrum of CL-LCDs-4 **DMSO-d_6**

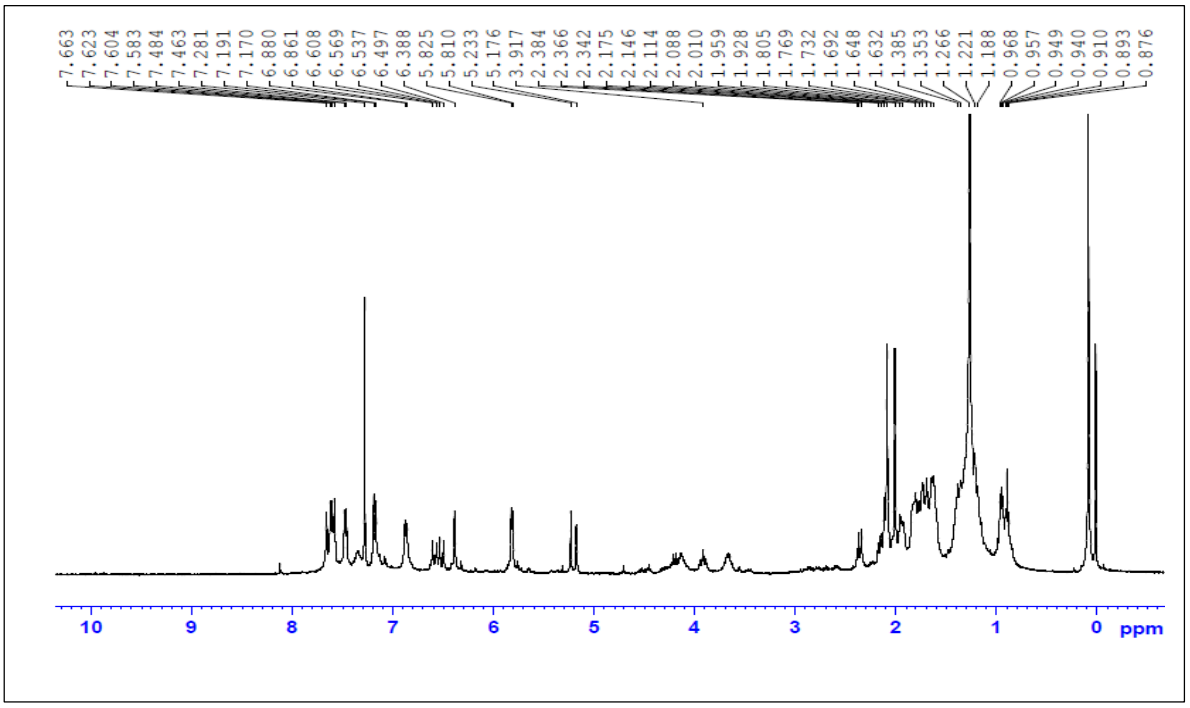

Spectrum 5.11: FT-IR spectrum Methotrexate loaded CL-LCDs

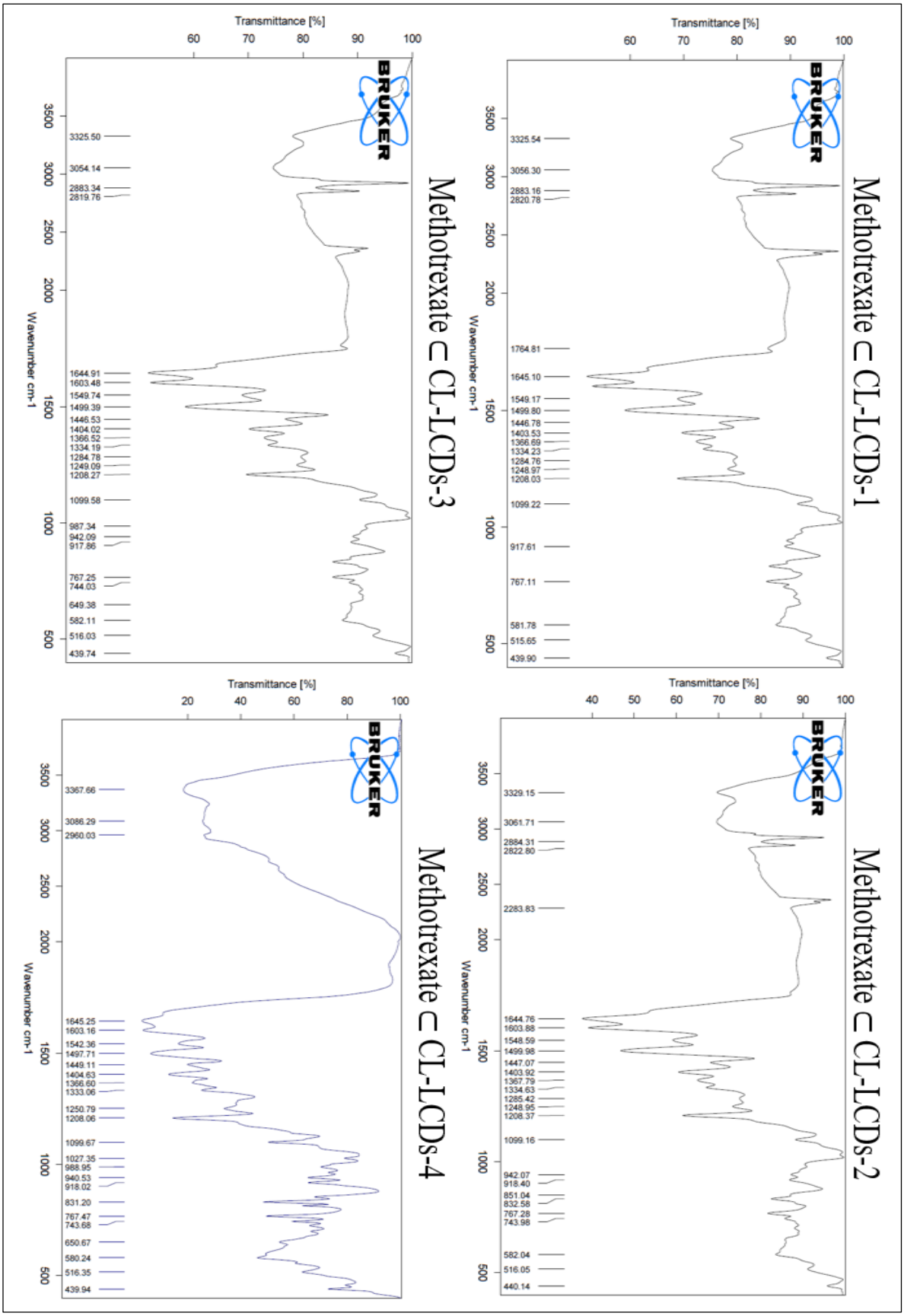

5.5 References

1 X. Xu, R. Ray, Y. Gu, H. J. Ploehn, L. Gearheart, K. Raker, W. A. Scrivens, *J. Am. Chem. Soc.*, 2004, **126**, 12736–12737.

2 Y. Yan, J. Gong, J. Chen, Z. Zeng, W. Huang, K. Pu, J. Liu, P. Chen, *Adv. Mater.*, 2019, **31**, 1–22.

3 J. Liu, Y. Geng, D. Li, H. Yao, Z. Huo, Y. Li, K. Zhang, S. Zhu, H. Wei, W. Xu, J. Jiang, B. Yang, *Adv. Mater.*, 2020, **32**, 1–9.

4 K. Jiang, Y. Wang, X. Gao, C. Cai, H. Lin, *Angew. Chemie Int. Ed.*, 2018, **57**, 6216–6220.

5 C. Hu, M. Li, J. Qiu, Y. P. Sun, *Chem. Soc. Rev.*, 2019, **48**, 2315–2337.

6 M. L. Liu, B. Bin Chen, C. M. Li, C. Z. Huang, *Green Chem.*, 2019, **21**, 449–471.

7 S. Zhu, Y. Song, X. Zhao, J. Shao, J. Zhang, B. Yang, *Nano Res.*, 2015, **8**, 355–381.

8 V. C. Hoang, K. Dave, V. G. Gomes, *Nano Energy*, 2019, **66**, 104093.

9 Z. Zhang, G. Yi, P. Li, X. Zhang, H. Fan, Y. Zhang, X. Wang, C. Zhang, *Nanoscale*, 2020, **12**, 13899–13906.

10 F. Yuan, Y. K. Wang, G. Sharma, Y. Dong, X. Zheng, P. Li, A. Johnston, G. Bappi, J. Z. Fan, H. Kung, B. Chen, M. I. Saidaminov, K. Singh, O. Voznyy, O. M. Bakr, Z. H. Lu, E. H. Sargent, *Nat. Photonics*, 2020, **14**, 171–176.

11 Disha, P. Kumari, M. K. Patel, P. Kumar, M. K. Nayak, *Biosensors*, 2022, 12, 1-12.

12 M. Ghirardello, R. Shyam, X. Liu, T. Garcia-Millan, I. Sittel, J. Ramos-Soriano, K. M. Kurian, M. C. Galan, *Nanoscale Adv.*, 2022, **4**, 1770–1778.

13 C. Rao, S. Khan, N. C. Verma, C. K. Nandi, *ChemBioChem*, 2017, **18**, 2385–2389.

14 F. Wen, P. Li, H. Meng, H. Yan, X. Huang, H. Cui, W. Su, *Photodignsis Photodyn. Ther.*, 2022, **39**, 103033.

15 I. Singh, R. Arora, H. Dhiman, R. Pahwa, *Turkish J. Pharm. Sci.*, 2018, **15**, 219–230.

16 S. Anwar, H. Ding, M. Xu, X. Hu, Z. Li, J. Wang, L. Liu, L. Jiang, D. Wang, C. Dong,

M. Yan, Q. Wang, H. Bi, *ACS Appl. Bio Mater.*, 2019, **2**, 2317–2338.

17 F. J. C. Mujica, L. G. Hernandez, S. C. Lopez, M. C. Lopez, M. A. C. Lopez, D. R. Contreras, A. P. Rodriguez, J. P. P. Caravaca, A. P. Rodriguez, J. G. D. Gonzalez, L. H. Tabares, O. A. D. Fuentes, E. Prokhorov, N. T. Figueredo, E. Reguera, L. F. D. Garcia, *J. Appl. Phys.*, 2021, **129**, 163301.

18 J. B. Essner, G. A. Baker, *Environ. Sci. Nano*, 2017, **4**, 1216–1263.

19 R. Xie, Z. Wang, W. Zhou, Y. Liu, L. Fan, Y. Li, X. Li, *Anal. Methods*, 2016, **8**, 4001–4006.

20 A. Sharma, J. Das, *J. Nanobiotechnology*, 2019, **17**, 1–24.

21 S. Cong, K. Liu, F. Qiao, Y. Song, M. Tan, *Methods*, 2019, **168**, 76–83.

22 F. Yan, Y. Jiang, X. Sun, Z. Bai, Y. Zhang, X. Zhou, *Microchim. Acta*, 2018, 185, 1-34.

23 U. Baruah, M. J. Deka, D. Chowdhury, *RSC Adv.*, 2014, **4**, 36917–36922.

24 S. Shishodia, V. Rimal, P. K. Srivastava, *Appl. Nanosci.*, 2021, **11**, 1691–1706.

25 L. Ai, H. Liu, R. Liu, H. Song, Z. Song, M. Nie, G. I. N. Waterhouse, S. Lu, *Sci. China Chem.*, 2022, **65**, 2274–2282.

26 K. Gao, Y. Guo, Q. Niu, L. Han, L. Zhou, L. Wang, *Sensors Actuators B Chem.*, 2018, **262**, 298–305.

27 I. P. J. Lai, S. G. Harroun, S. Y. Chen, B. Unnikrishnan, Y. J. Li, C. C. Huang, *Sensors Actuators B Chem.*, 2016, **228**, 465–470.

28 J. Dilag, H. Kobus, Y. Yu, C. T. Gibson, A. V. Ellis, *Polym. Int.*, 2015, **64**, 884–891.

29 G. Kalaiyarasan, M. Veerapandian, G. Jebamercy, K. Balamurugan, J. Joseph, *ACS Biomater. Sci. Eng.*, 2019, **5**, 3089–3099.

30 S. Murugesan, V. Srinivasan, D. K. Lakshmanan, M. R. Venkateswaran, S. Jayabal, M. S. A. Muthukumar Nadar, A. Kathiravan, M. Asha Jhonsi, S. Thilagar, S. Periyasamy, *Food Funct.*, 2021, **12**, 5038–5050.

31 M. Z. Fahmi, A. Haris, A. J. Permana, D. L. Nor Wibowo, B. Purwanto, Y. L. Nikmah,

A. Idris, *RSC Adv.*, 2018, **8**, 38376–38383.

32 A. S. Krishna, C. Radhakumary, S. S. Priya, R. M. Ramesan, S. Kunnatheeri, *RSC Adv.*, 2016, **6**, 56313–56318.

33 M. S. Ramasamy, S. S. Mahapatra, H. J. Yoo, Y. A. Kim, J. W. Cho, *J. Mater. Chem. A*, 2014, **2**, 4788–4794.

34 N. Deirram, C. Zhang, S. S. Kermaniyan, A. P. R. Johnston, G. K. Such, *Macromol. Rapid Commun.*, 2019, **40**, 1–23.

35 B. T. Hoan, P. D. Tam, V. H. Pham, *J. Nanotechnol.*, 2019, **2019**, 1-10.

36 G. Kalaiyarasan, C. Hemlata, J. Joseph, *ACS Omega*, 2019, **4**, 1007-1014.

37 A. E. B. Yassin, M. D. Khalid Anwer, H. A. Mowafy, I. M. El-Bagory, M. A. Bayomi and I. A. Alsarra, *Int. J. Med. Sci.*, 2010, **7**, 398–408.

38 K. Nagahama, T. Utsumi, T. Kumano, S. Maekawa, N. Oyama and J. Kawakami, *Sci. Rep.*, 2016, **6**, 1–14.

39 E. M. Schneider, A. Bartsch, W. J. Stark, R. N. Grass, J. Chem. Edu., 2019, 96, 540-545.

40 P. Roy, A. P. Periasamy, C. Chuang, Y. R. Liou, Y. F. Chen, J. Joly, C. Te Liang, H. T. Chang, *New J. Chem.*, 2014, **38**, 4946–4951.

41 M. He, J. Zhang, H. Wang, Y. Kong, Y. Xiao, W. Xu, Nanoscale Res. Lett., 2018, 13, 1-7.

42 W. Zhang, D. Dai, X. Chen, X. Guo, J. Fan, *Appl. Phys. Lett.*, 2014, **104**, 1-4.

43 S. Zhu, Y. Song, X. Zhao, J. Shao, J. Zhang, B. Yang, *Nano Res.*, 2015, **8**, 355–381.

44 J. Zhang, H. Wang, Y. Xiao, J. Tang, C. Liang, F. Li, H. Dong, W. Xu, *Nanoscale Res. Lett.*, 2017, **12**, 1–7.

45 J. K. Patra, G. Das, L. F. Fraceto, E. Vangelie, R. Campos, P. Rodriguez, L. Susana, A. Torres, L. Armando, D. Torres, R. Grillo, *J. Nanobiotechnology*, 2018, **16**, 1–33.

46 A. K. Bajpai, J. Choubey, *J. Macromol. Sci. Pure Appl. Chem.*, 2005, **42**, 253–275.

47 B. R. Giri, J. S. Kim, J. H. Park, S. G. Jin, K. S. Kim, F. Din, H. G. Choi, D. W. Kim, *Pharmaceutics*, 2021, **13**, 1-14.

48 C. L. Porras, P. C. Alcantar, V. E. Sol, M. Z. S. Leos, *Polymers*, 2019, **12**, 1–21.

49 H. M. Tawfeek, W. Faisal, G. M. Soliman, *Pharm. Dev. Technol.*, 2017, **23**, 496–503.

50 H. M. Tawfeek, Y. A. Hassan, M. F. Aldawsari, M. H. Fayed, *Pharmaceuticals*, 2020, **13**, 1–17.

51 P. Suresh, M. M. S. Bekhit, H. P. Veedu, S. Alshehri, S. C. Nair, S. I. Bukhari, V. Viswanad, E. I. Taha, R. K. Sahu, M. M. Ghoneim, I. Elbagory, *Nanomaterials*, 2022, 12, 1-16.

52 I. Todorovska, K. Dragarska, J. Bogdanov, *Chem. Proc.*, 2022, **12**, 1-10.